Effective elastic thickness of Africa and its relationship to other proxies for lithospheric structure and surface tectonics

M. Pérez-Gussinyé[1], M. Metois[2], M. Fernández[3], J. Vergés[3], J. Fullea[3], A.R. Lowry[4]

[1] Dept. of Earth Sciences, Royal Holloway, University of London
[2] Ecole Normale Supérieure de Lyon, France
[3] Institute of Earth Sciences "Jaume Almera", Spanish Research Council
[4] Dept. of Geology, Utah State University

Abstract

Detailed information on lateral variations in lithospheric properties can aid in understanding how surface deformation relates to deep Earth processes. The effective elastic thickness, T_e, of the lithosphere is a proxy for lithospheric strength. Here, we present a new T_e map of the African lithosphere estimated from coherence analysis of topography and Bouguer anomaly data. The latter data set derives from the EGM 2008 model, the highest resolution gravity database over Africa, enabling a significant improvement in lateral resolution of T_e. The methodology used for T_e estimation improves upon earlier approaches by optimally combining estimates from several different window sizes and correcting for an estimation bias term. Our analysis finds that T_e is high, ~ 100 km, in the West African, Congo, Kalahari and Tanzania cratons. Of these, the Kalahari exhibits the lowest T_e. Based in part on published seismic and mineral physics constraints, we suggest this may reflect modification of Kalahari lithosphere by anomalously hot asthenospheric mantle. Similarly, the Tanzania craton exhibits relatively lower T_e east of Lake Victoria, where a centre of seismic radial anisotropy beneath the craton has been located and identified with a plume head, thus suggesting that here too, low T_e reflects modification of cratonic lithosphere by an underlying hot mantle. The lowest T_e in Africa occurs in the Afar and Main Ethiopian rifts, where lithospheric extension is maximum. In the western Ethiopian plateau a local T_e minimum coincides with published images of a low P and S seismic velocity anomaly extending to $\sim$400 km depth. Finally, the Darfur, Tibesti, Hoggar and Cameroon line volcanic provinces are characterised by low T_e and no deep-seated seismic anomalies in the mantle. Corridors of relatively low T_e connect these volcanic provinces to the local T_e minima within the western Ethiopian plateau. We interpret the low T_e to indicate thinner lithosphere within the corridors than in the surrounding cratons. We speculate that these corridors may provide potential conduits for hot asthenospheric material to flow from the western Ethiopian plateau to the volcanic provinces of central and western Africa.

1. Introduction

How surface deformation is related to thickness and composition of the lithosphere is not well understood. A common view is that repeated episodes of extension and compression avoid old, thick and rigid cratonic interiors, instead focusing in off-craton mobile belts where lithosphere is younger, thinner and weaker. However, this is not always the case and several cratons show evidence of modification by plume-related magmatism (e.g. South Africa; Griffin et al., 2003) or extreme thinning triggered by deep-seated recycling processes (e.g. North China craton; Menzies et al., 2007), leading in some cases to break-up (e.g. Labrador Sea; Tappe et al., 2007). Detailed, three-dimensional knowledge of lithospheric properties can aid in understanding how deformation is distributed across continents. Unfortunately, the most relevant properties (geotherm, rheology, and depth-dependent density variations) cannot be measured directly so must be inferred from proxies. These proxies are based on observations of petrology, geochemistry (Finnerty and Boyd, 1987), heat flow (e.g. Mareschal and Jaupart, 2004), seismic velocity (Priestley and Tilmann, 2009), seismic-anisotropy (e.g. Sebai et al. 2006), electrical conductivity (Jones, 1999) and modelling of

potential fields, topography, surface heat flow and seismic velocity data (Fullea et al., 2007; Fernandez et al, 2009). For an extensive review on some of these methods see Eaton et al. (2008).

The effective elastic thickness, T_e, is an alternative measure of lithospheric properties. The effective elastic thickness corresponds to the thickness of an idealized elastic beam that would bend similarly to the actual lithosphere under the same applied loads (Watts, 2001). Because, in practice, the layers composing the lithosphere fail anelastically in both brittle and ductile fashion, T_e actually represents an integral of the bending stress within limits imposed by the rheology of the lithosphere (Burov and Diament, 1995). Since T_e parameterizes lithospheric strength it has been commonly used to understand the relationship between tectonic styles and lithospheric rheology in various tectonic settings. Various researchers have examined, for example, the relationship of fault length and basin width to lithospheric rigidity in extensional settings (e.g. Ebinger et al., 1999), the relationship of the style of fold-and thrust belt tectonics to rigidity of foreland lithosphere (e.g. Watts et al., 1995), and vertical motions in response to loading or unloading during sedimentation, glaciation, de-glaciation, and erosion (e.g. Watts, 1982; Whitehouse et al., 2006).

Here we demonstrate how modern spectral techniques can recover detailed variations in T_e over continental scales, thus providing a measure of the lithosphere's lateral strength variations and further insight into the relationship between surface tectonics and Earth's deep interior. Sensitivity analysis of T_e indicates that it primarily depends on parameters of power law creep, i.e., temperature, crustal thickness, other lithologic variations, and to a lesser degree strain rate (Lowry and Smith, 1995; Burov and Diament, 1995; Lowry et al., 2000; Brown and Phillips, 2000). Thus T_e can be interpreted as a proxy mapping variations in lithospheric rheology, and because it depends strongly on temperature and lithology it exhibits structure similar to that of seismic velocity variations. Although T_e does not represent an actual depth to the base of the mechanical lithosphere, its spatial variations reflect relative lateral variations in lithospheric mechanical thickness.

In this study we present a new map of spatial variations of T_e in Africa and relate it to the tectonic processes that have shaped the continent. Africa is an ideal natural laboratory to examine relationships between surface deformation, lithospheric structure and the underlying convecting interior, as it has been practically stationary within the hotspot reference frame during the last 30 Myr (Morgan, 1983), leading to long-lived interactions between hot upwellings in the mantle and the lithosphere (Burke, 1996). Also, and perhaps because of Africa's stationarity over asthenospheric thermal anomalies in several locations, some cratonic blocks appear to be in early stages of modification. Examples include the Kalahari and Tanzania cratons, the latter of which is presently undergoing extension (Calais et al., 2008; Ebinger et al., 1997).

In the following sections we first describe key observations of African tectonics relevant to this study. Subsequently we describe the data, new improvements to methodology that are implemented for this particular study, and resulting resolution of T_e mapped from coherence analysis based on tests with synthetic topography and gravity anomaly data. In an appendix, we address potential effects of correlated loads on T_e estimates in Africa. Finally, we discuss the relationship between lateral variations of T_e in Africa and its lithospheric and asthenospheric structure by comparison with other proxies for lithospheric properties. We also discuss how the lithospheric structure interpreted from our T_e analysis relates to surface tectonism in Africa.

2. An outline of African tectonics

The African continent is predominantly underlain by Precambrian basement. The largest cratonic blocks of the continent are the West African, the Congo, Kalahari and Tanzania (Figure 1). These cratons were amalgamated during the Pan African orogeny to create the Gondwana supercontinent. Break-up of Gondwana occurred in the Mesozoic. Along its southeast coast, South Africa experienced Karoo flood basalt volcanism ~183 Ma, which initiated the separation of Madagascar, Antarctica and India from Africa (Storey, 1995). On the west coast, late Jurassic to Early Cretaceous initiation of the South Atlantic appears to relate to activity of the Tristan da Cunha hotspot (Storey, 1995). Rifting in the proto-Central Atlantic region began in the Late Jurassic and appears to relate to activity of the St. Helena hotspot. Central Atlantic rifting is affiliated with a major phase of intra-continental extension in the West Africa, Central Africa and Anza rift systems (see Figure 1 of Guiraud and Maurin 1992). Separation of South America and Africa was achieved 100-105 Ma (Nurnberg and Muller, 1991).
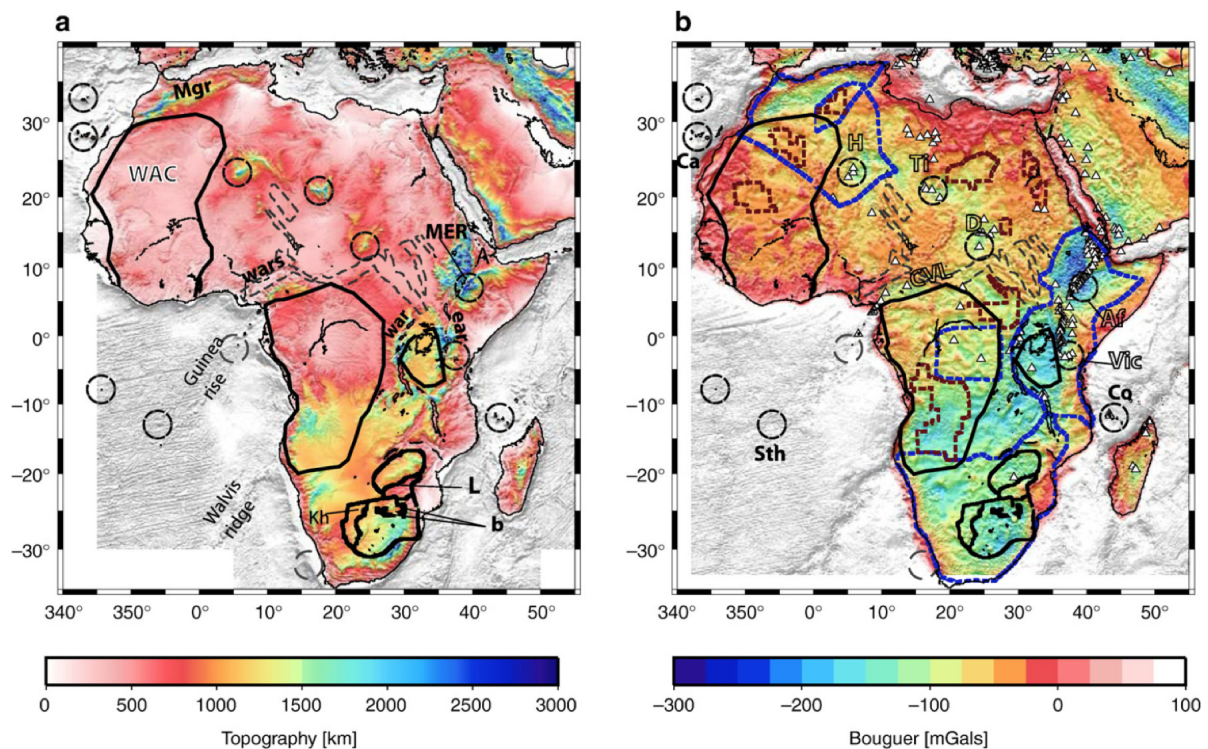
———————————————————

Figure 1. Topography (a) and gravity (b) of Africa overlain by main tectonic units relevant to this study and Cenozoic volcanism (b). Main cratons: **WAC**: West African craton, **CC**: Congo craton, **T**: Tanzania craton. The Kalahari craton in South Africa is formed by the following units: **L**: Limpopo belt, **Kh**: Kheis belt, **K**: Kapvaal craton, **Z**: Zimbawe craton, **b**: is the extent of the surface exposure of the ~2.1Ga old Bushveld magmatic complex. Dashed thin lines indicate the extent of the Mesozoic western and central African rifts, labelled **wars** and **cars**, respectively. Cenozoic units: **MER**: Main Ethiopian rift, **A**: Afar, **war**: western branch of the East African rift, **ear**: eastern branch of the East African rift. **H**: Hoggar, **Ti**: Tibesti, **D**: Darfur, **CL**: Cameroon line are intra-continental volcanic provinces in Africa. **Sth**: Saint Helena hot-spot with its hot-spot track: Guinea rise. Walvis ridge is the hot-spot track of the Tristan da Cunha hot-spot.

———————————————————

Renewed volcanism starting ~45 Ma occurred simultaneously in several regions of Africa, including the Hoggar, Tibesti, Darfur, Cameroon line, and East Africa (Ebinger and Sleep, 1998; Figure 1). The largest volumes of magma were emplaced over the Ethiopian and East African plateaus at ~31-29 Ma, simultaneous with the initiation of extension in the Red Sea and Gulf of Aden (Hofmann et al., 1997), while rifting in East Africa is spatially variable with onset of 30 Ma in Afar, and ~1 Ma in NE Tanzania (Wolfenden et al., 2004). The

3

initiation of Cenozoic volcanism in Africa is coeval with uplift of the South and Eastern African plateaus, which today are ~1 km high (Burke, 2009). These anomalously high elevations are known as the African superswell (Nyblade and Robinson, 1994) and have variously been attributed to the presence of a shallow thermal anomaly beneath the South African lithosphere (Li and Burke, 2006; Wang et al., 2008) or to dynamic topography arising from plumes generated by thermochemical convection, and evidenced by a shear wave seismic velocity anomaly in the lower mantle under southern Africa (Lithgow-Bertelloni and Silver, 1998).

Finally, Africa has remained relatively stationary within the hotspot reference frame for the last 30 Myr (Morgan, 1983). Some have claimed that this stationarity has led to the basin and swell topography of Africa (Burke, 1996), while others dispute this. In any case, stationarity of Africa has promoted long-lived interaction of the lithosphere with the convecting interior.

3. Data

To calculate the effective elastic thickness we use coherence analysis of the topography and Bouguer anomaly (Forsyth, 1985). We generate the Bouguer anomaly gravity data by first dividing Africa into 3 different areas from south to north and projecting each of them into cartesian coordinates. We calculated terrain corrections using the ETOPO2 digital elevation model and added these to free-air gravity data from EGM2008 (Pavlis et al., 2008). The Bouguer correction procedure applied the complete terrain correction (i.e. Bullard A, B and C corrections) using the FA2BOUG software (Fullea et al., 2008). EGM2008 provides a free-air gravity database of ~20 km mean resolution that exploits all of the latest data and modelling for both land and marine areas worldwide. In Africa, available terrestrial gravity data used to construct the EGM2008 model do not cover the whole continent, but covers the whole of the East African rift from Ethiopia to Malawi. Data coverage is good in some regions of northwestern Africa (e.g., Morroco and Algeria), the central part of the Democratic Republic of Congo and all of southern Africa including South Africa, Botswana, Namibia, Zimbabwe and Mozambique (Pavlis et al., 2008). In some areas such as Angola and parts of Libya and Egypt, data are unavailable and in the rest of Africa proprietary data exists which could not be publicly released. In these areas synthetic gravity anomalies were generated using techniques that combine GRACE, lower-resolution gravity, and terrain corrections to create a 2.5'x2.5' mean anomaly dataset that protected the proprietary nature of the original data, while providing a mean anomaly with an adequate high-frequency component (see Pavlis et al., 2008). Maps showing the distribution of the data in Africa can be found in Pavlis et al. (2008). The topography and Bouguer anomaly data sets used for our analysis are shown in Figure 1.

4. Methods: attenuation of windowing effects on recovered T_e.

The coherence function relating the topography and Bouguer anomaly, commonly known as Bouguer coherence, gives information on the wavelength band over which topography and Bouguer anomaly are correlated. To estimate T_e we compare the observed coherence curve with coherence functions predicted for a range of T_e values. For each given T_e, we calculate via deconvolution the surface and sub-surface loads and compensating deflections that reproduce exactly the observed topography and gravity anomaly, an approach first described by Forsyth (1985). We then calculate a predicted coherence assuming that surface loads (atop the lithosphere) and subsurface loads (within or below the lithosphere) are statistically uncorrelated (Forsyth, 1985). The deconvolution requires information on the density structure of the crust, which we deduced from CRUST 2.0 (Laske et al., 2000). The T_e that minimizes

the difference between predicted and observed coherence is the assigned T_e for an analyzed area.

To obtain a map of the lateral variation we first estimate T_e within moving windows. As the resulting T_e estimate depends on window size (Pérez-Gussinyé et al., 2004), we use three different window sizes. We then correct the results obtained with each window for the downward bias introduced by windowing (see below). Finally, we merge the results obtained from the three windows in order to recover optimally both the small-scale variations best resolved by smaller windows and high T_e which is most robustly returned by the largest window. This approach represents a significant departure from our earlier methodology (e.g., Pérez-Gussinyé et al., 2009). In what follows we explain in more detail these steps.

Firstly, to recover spatial variations in T_e we divide the analysis area into overlapping windows. In each window the coherence is calculated and inverted assuming that T_e is spatially constant. The centre of each window is moved 50 km for each new estimate. The effect of calculating T_e within a finite-aperture window is to limit the maximum wavelength of the gravity and topography that can be recovered. Hence, if T_e were spatially constant, a larger window would more accurately recover T_e because the flexural wavelength would be better sampled.
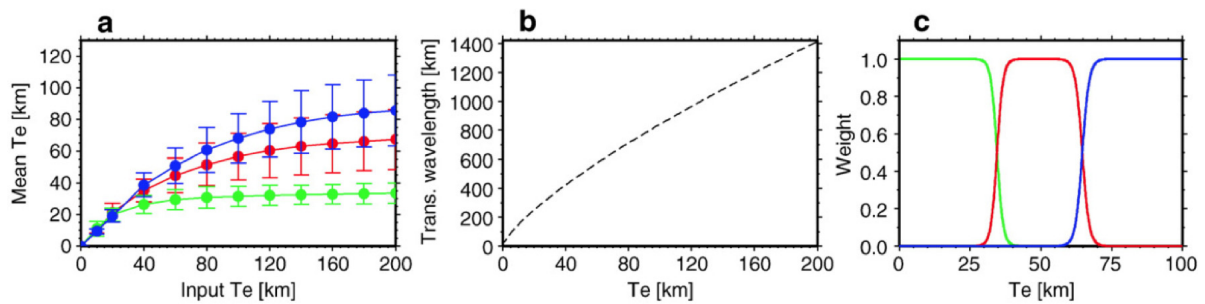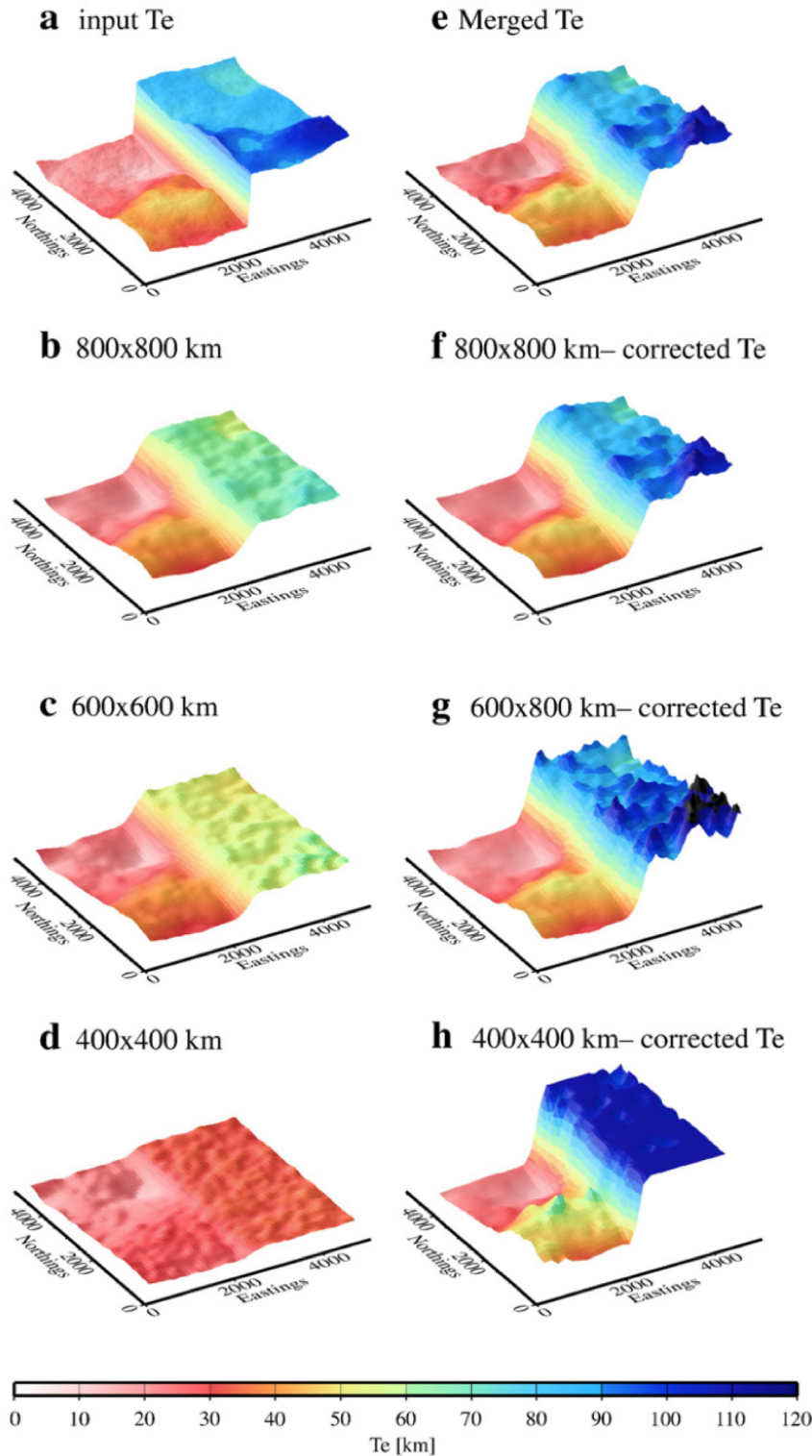
_____

Figure 2. **a)** Mean recovered T_e, T_{e_mean} and its standard deviation, ΔT_{e_std}, resulting from doing 100 experiments with synthetic topography and gravity generated with a spatially constant input Te. Three windows for analysis are used, 400x400 km: green line, 600x600 km windows: red line, 800x800 km windows: blue line. Higher input T_e yields larger downward biased when recovered with small windows than with large windows. **b)** Coherence transition wavelength as a function of T_e, calculated following Kirby and Swain (2008). The transition wavelength is defined as the wavelength at which the coherence is 1/2 and can be viewed as a measure of the wavelength at which the transition from uncompensated (where coherence equals zero) to isostatically compensated loads (where coherence equals 1), occurs for a given T_e. **c)** Weights, w_{win}, applied to the results obtained with each window. The weights are Gaussian curves, centred on T_{ec} mid-way between the maximum T_e recoverable with a given window and the maximum T_e recoverable with the next smaller window. We assume the maximum T_e that can be recovered with a given window corresponds to that with the maximum transitional wavelength that fits within the window (Figure 2b). For the smallest and largest windows, T_e lower and higher, respectively, than T_{ec} have a weight of 1.

_____

The coherence transition wavelength is defined as the wavelength at which the coherence is 0.5 and can be viewed as an approximation of the wavelength at which the transition from uncompensated (where coherence equals zero) to isostatically compensated loads (where coherence equals 1) occurs for a given T_e. Simons and van der Hilst (2003) give an estimate of the "coherence transition wavelength" (a typo in their equation is corrected in Kirby and Swain, 2008) and show that it depends primarily on T_e with a secondary dependence on the ratio of subsurface to surface loads, f. For $f = 1$, the transition wavelength of $T_e \sim 37$ km is 400 km, that of $T_e \sim 63$ km is 600 km and that of $T_e \sim 93$ km is 800 km (Figure 2b). Therefore windows of 400x400 km, 600x600 km and 800x800 km can recover T_e only up to

approximately those values. This effect is shown in Figure 2. There the mean T_e, T_e^{mean}, and the standard deviation, ΔT_e^{std}, from simulations with 100 synthetic topography and Bouguer anomaly data sets generated using spatially constant input T_e, T_e^{input}, of 10, 20, 40, 60, 80, 100, 120 140, 160 and 200 km are shown. The figure shows that as the input T_e increases for a given analysis window, both the downward bias error and the estimate uncertainty increases. As the window size decreases this effect occurs at lower T_e, such that when T_e is spatially constant, larger windows produce more accurate estimates (Swain and Kirby, 2003; Pérez-Gussinyé et al., 2004).

Figure 3. Recovery of a spatially variable input T_e (shown in **a**). Figures **b** to **d** show recovery of T_e with different window sizes. Figure **f** to **h** show recovered T_e using the correction curves shown in Figure 2a (see Section 4). Note that in **h**, the recovered T_e in the area where T_e is highest is often significantly overestimated and so has been limited to 110 km for plotting purposes. Figure **e** shows T_e after merging the corrected results obtained with the 3 windows (**e** to **f**). See Section 4 for the procedure followed in merging.

That the downward bias in T_e is greater for smaller windows can also be appreciated in Figure 3 where a structure consisting of a steep T_e gradient separating two broad areas of low and high T_e is used as input for the generation of 100 synthetic Bouguer anomaly and topography data sets (Figure 3a). Figures 3b, c and d show that as the window size for analysis decreases, the downward bias of the recovered T_e increases, consistent with the results shown in Figure 2. For detailed information on how the synthetic data was generated see Kirby and Swain (2008).

To remove the bias related to windowing, we apply a correction factor based on functions that reproduce the variation of T_e^{mean}, with T_e^{input}, i.e. $T_e^{mean} = f_{win}(T_e^{input})$, where the sub-index *win* indicates that the function differs for each window (see Figure 2a). These functions were constructed by fitting a spline function to T_e^{mean}. The correction factor is calculated by inverting f_{win} to obtain T_e^{input} as a function of the recovered T_e^{rec}, $T_e^{input} = f_{win}^{-1}(T_e^{rec})$, where the superscript -1 denotes inverse. Note that T_e^{mean} and T_e^{rec} differ in that T_e^{mean} is the mean value of 100 recovered T_e^{rec} for a given input T_e, T_e^{input}. Thus T_e^{mean} can only be obtained from synthetic data, where many topography and gravity data sets can be generated with identical T_e^{input}. For real data we only have one recovered T_e^{rec} at each geographical location. Thus in synthetic data, the correction factors are applied to the mean value T_e^{mean}, while in real data they are applied to a single realization of T_e^{rec}. This bias correction was previously applied to South America for the 600x600 km window (Pérez-Gussinyé et al., 2009). Here we additionally show the result of applying a different correction to analysis windows of different sizes (Figures 3f to h). Small windows capture the abrupt gradients in T_e better than larger ones, but have larger uncertainties and the estimates saturate at a lower threshold of T_e (compare Figure 3h to 3f). Here, "saturation" refers to the fact that the correction curve becomes flat for values larger than a given threshold. For example, for the 400x400 km window, the correction curve becomes very flat for $T_e^{mean} > \sim 37$ km (Figure 2a), and hence estimates larger than ~37 km correspond to a wide range of T_e^{input}, eventually leading to an overestimation of the input T_e upon correction. Note that because the bias-corrected T_e for the 400x400 km window can be significantly overestimated when the recovered T_e is near the saturation level, estimates have been limited to 110 km for plotting purposes.

As a final step we generate a T_e map that combines the information content regarding abrupt T_e gradients recovered by small windows and the more reliable information on high T_e recovered by the larger windows. This is done by calculating a weighted average of the T_e estimates from each of three windows. Figure 2c shows the weight scheme, which is designed so that estimates from small windows predominate when the recovered T_e^{rec} is low and large window estimates prevail when T_e^{rec} is high. The merged T_e, T_e^{merged}, is given by:

$$T_e^{merged} = \frac{1}{NORM} \sum_{i=1}^{nwin} w_i f_i^{-1}(T_e^{rec})$$

$$NORM = \frac{1}{\sum_{i=1}^{nwin} w_i}$$

where w_i are the weights assigned to each of the windows (Figure 2c). These are defined as Gaussian curves centred on T_e^{cen}, located mid-way between the maximum T_e recoverable within the given window and the maximum T_e recoverable within the next smaller window. We assume that the maximum recoverable T_e corresponds to that having the maximum transitional wavelength that fits within the window (e.g. 37, 63 and 93 km for 400x400 km, 600x600 km and 800x800 km windows, respectively, Figure 2b). The smallest and largest windows are given a weight of 1 for T_e lower and higher, respectively, than T_e^{cen}. The bandwidth of the Gaussian curve was chosen so the transition from one window to the next would be smooth. We tested a range of bandwidths and the difference in resulting merged maps is not appreciable.
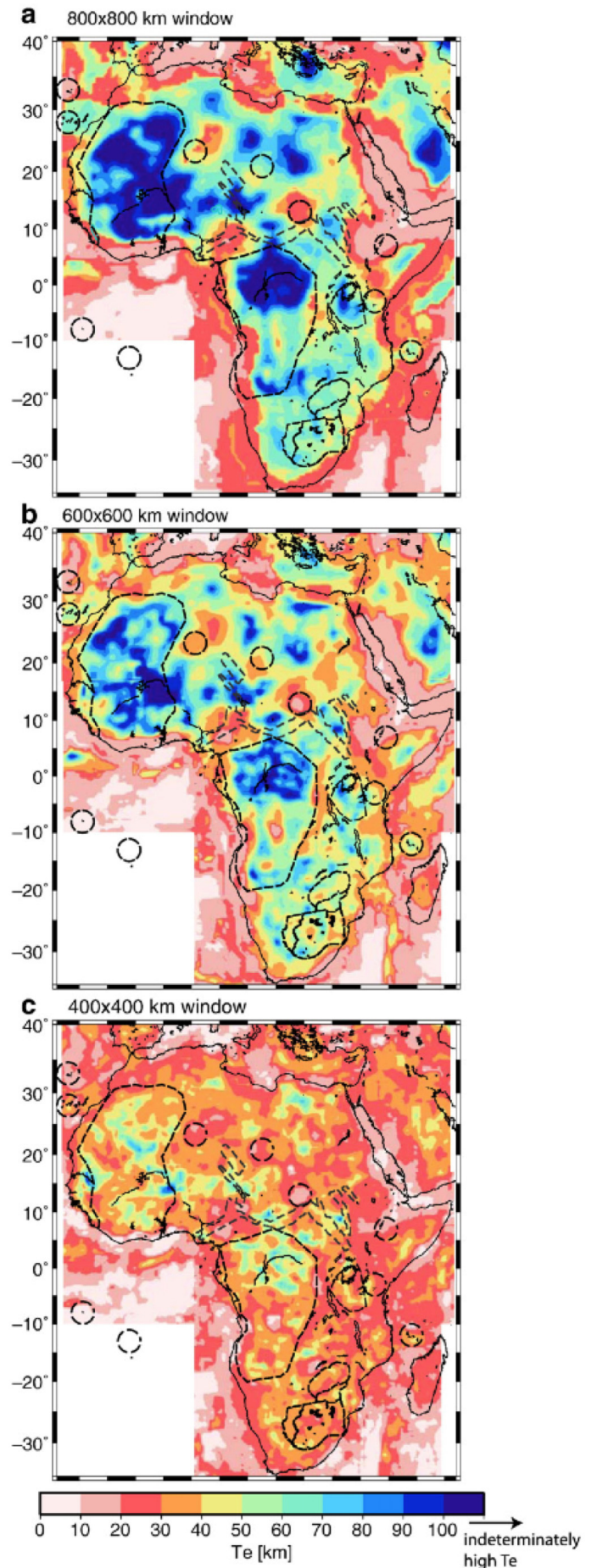
Figure 3e depicts T_e after merging the bias-corrected T_e from the three windows. The final T_e structure retains the primary characteristics of the largest window, but it better resolves the sharp gradient between low and high T_e areas and the short wavelength variations in T_e than does the map using only the largest window, thus reflecting the influence of the smaller size windows.

———————————————

Figure 4. a to **c** show T_e of Africa for 3 different window sizes overlain by main cratons, hotspots and west and central African rift systems. The maximum T_e recovered for the smallest window is much lower than that for a larger window. This is consistent with a windowing-related downward bias, which is largest for the smallest window, as shown in Figures 2 and 3.

———————————————

5. Results

Figure 4 shows the estimates of T_e in Africa using three different window sizes. As with the synthetic data, the three maps vary in the absolute values recovered and in the small short wavelength variation in T_e. Nonetheless, all maps exhibit highest T_e over the West African and Congo cratons followed by the Tanzania and South-African cratons. The lowest T_e occurs over the axis of the main Ethiopian rift, with a T_e minimum over the Afar triangle (Figure 4). Intermediate T_e occurs over the western and eastern branches of the East African rift, and over the Hoggar, Tibesti and Darfur hot spots and the Cameroon volcanic line (see Figure 1 for location).
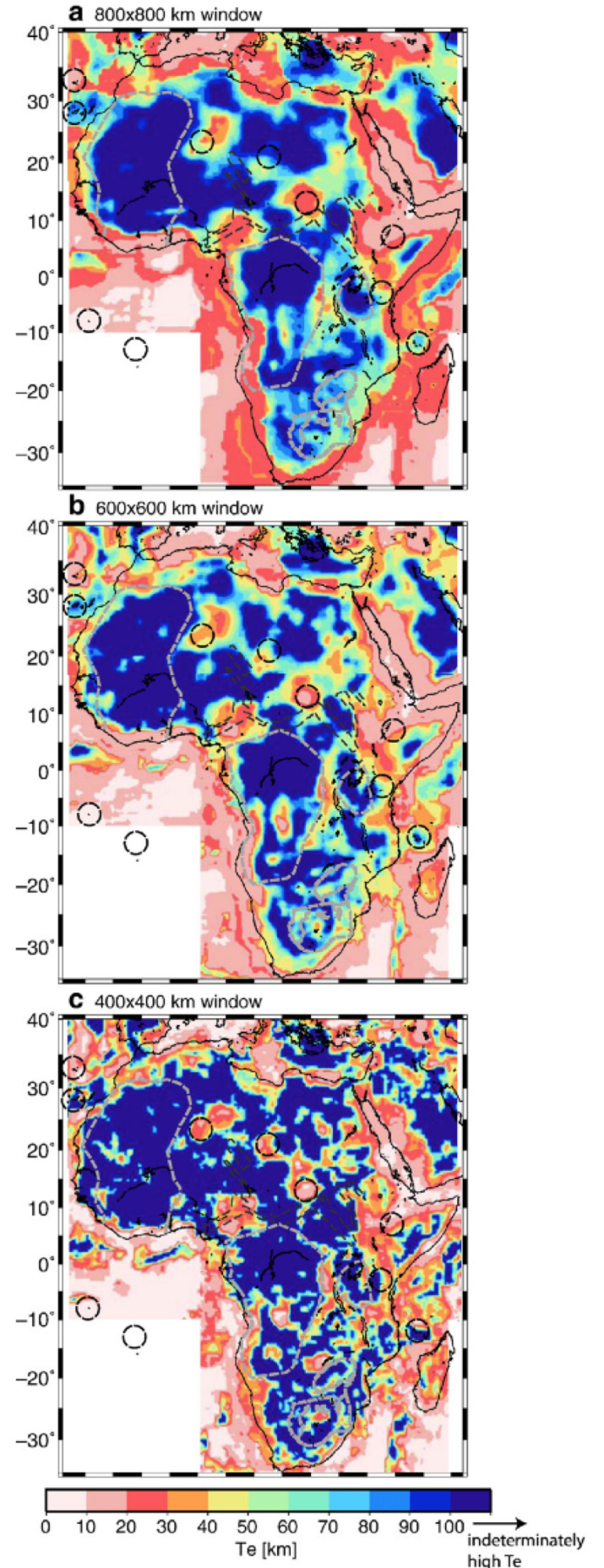
Interpretation of T_e estimates necessarily carries several caveats. A common concern is that T_e reflects a lithospheric equilibrium developed at the time of loading, suggesting that under some circumstances it may represent a "fossil" rheological state. If loading occurs when T_e is low and no subsequent mass redistribution occurs, there is no need for stress to re-equilibrate and isostatic analysis might yield a low estimate even after cooling and strengthening of the lithosphere. (A similarly "fossil" high T_e is implausible because load stress must re-equilibrate via flexure in a weakening lithosphere). However, while loading processes in oceans may be time-specific, surface processes of erosion and

a 800x800 km window

b 600x600 km window

c 400x400 km window

Te [km]

indeterminately high Te

deposition constantly redistribute continental surface mass loads. Reliable estimates of high ($\geq$ 100 km) T_e in cratonic regions (e.g., the North American Superior province, Kirby and Swain, 2009) are consistent with expectations for a modern rather than fossil thermal and compositional state, despite the fact that surface mass redistribution processes act at the lowest rates over cratons. This is why maps of T_e in continents are qualitatively similar to shear wave velocity maps that reflect modern-day lithospheric properties (Kirby and Swain, 2009; Pérez-Gussinyé et al., 2008; Audet et al., 2007), whereas such a relationship is not observed in oceanic lithosphere (Kalins and Watts, 2009).

_____

Figure 5. a to **c** show T_e of Africa for 3 different window sizes after correction for the downward bias related to windowing (see Section 4). Because bias correction may lead to unrealistically high estimates when T_e exceeds the saturation threshold for an 800 km window, we limit our colour scale to 100 km. Cratons, hotspots and west and central African rift systems are also shown.

_____

A second caveat is that Forsyth's (1985) coherence method assumes surface and subsurface loads are uncorrelated. Macario et al. (1995) showed that when correlation of initial surface and subsurface loading occurs, the T_e values estimated using Forsyth's (1985) deconvolution method can be biased. Kirby and Swain (in press) find that the real part of the complex Bouguer coherency indicates wavelengths for which initial load correlation occurs (see their Figure A2 and our Appendix A for definition of the coherency). In Appendix A we show that correlation of initial surface and subsurface loads occurs in western Africa near the East African and Main Ethiopian rifts and Afar, but that this correlation is limited to wavelengths < ~100 km. We also show in the appendix that load correlation at such short wavelengths does not bias our T_e estimates because the T_e transitional wavelength is much longer than the waveband over which correlation occurs. Correlation of surface and subsurface loads in the volcanic provinces of Africa probably relates to emplacement of volcanic edifices over subsurface magmatic intrusions.

Kirby and Swain's (in press) analysis emphasized another type of correlated loading specifically associated with basin deposition in very-low-relief cratonic regions. We did not attempt to evaluate the presence or absence of such load correlation in Africa, partly because most African cratons express significant topographic relief and partly because such analysis lies beyond the scope of this paper. However, we note that if such correlated loading occurs in Africa, its effect would be to bias T_e toward higher estimates in cratonic regions having extremely low relief (Kirby and Swain, in press).

After applying the windowing correction, the T_e maps look more similar, with consistently high T_e over cratonic areas and more abrupt T_e contrasts between low and high T_e regions than in the uncorrected maps (compare Figure 5 and 4). We limit the colour-scale to a maximum T_e of 100 km. Recovery degrades for higher T_e, so we consider values of >~100 km indeterminately high. Still, differences between the three maps persist. For example, small-scale features with relatively low T_e, such as those within the Kalahari craton, the fold belts around the Tanzania craton and the low T_e along the Ethiopian rift, are much more sharply defined with the smallest window as it introduces less spatial smoothing.
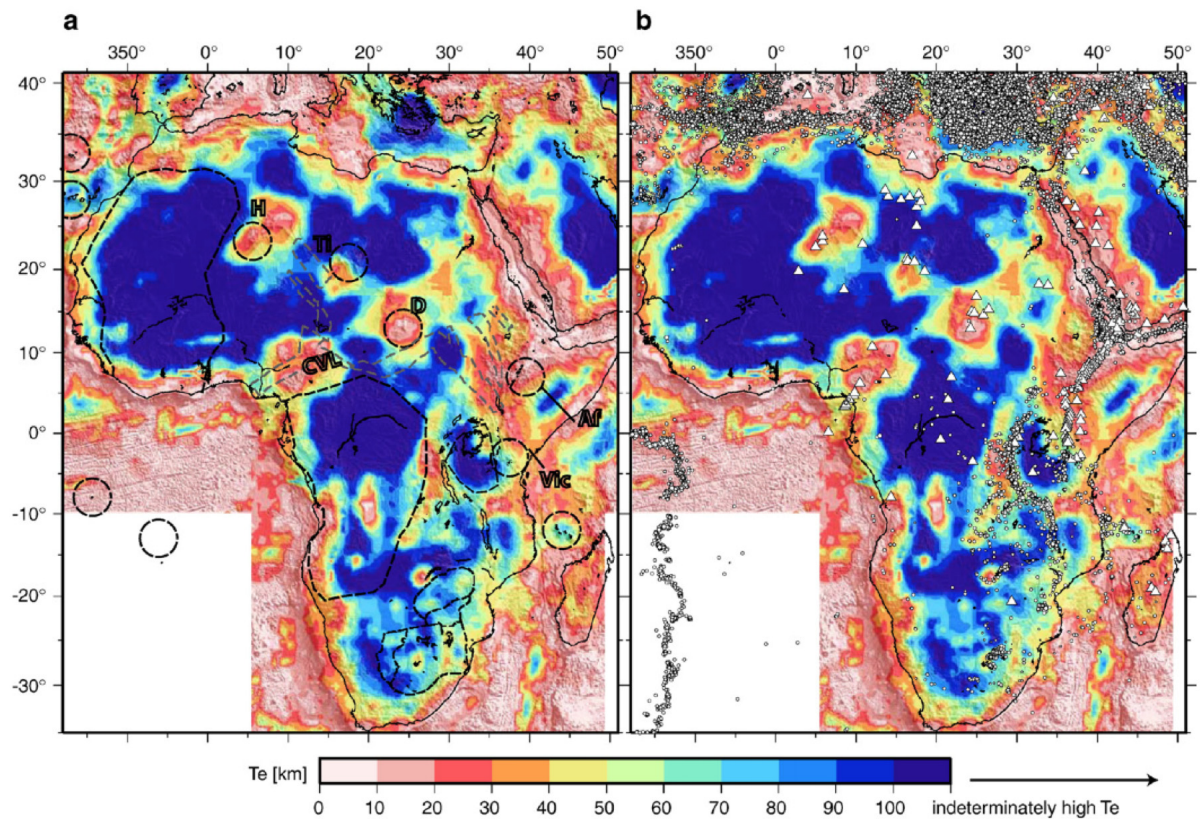

Figure 6. The final result after merging bias-corrected T_e from three different windows using the procedure explained in Section 4, with **a)** hypothesized hot-spots in the African plate (as proposed by Morgan and Phipps Morgan, 2007), cratons and west and African rift systems. CVL: Cameroon volcanic line, H, Ti and D are Hoggar, Tibesti and Darfur volcanic provinces. Af and Vic mark the proposed locations of Afar and Victoria hotspots. **b)** Merged and bias-corrected T_e overlain by Cenozoic volcanoes and earthquakes with magnitude M_b > 4.5. Note the general correspondence between low T_e, volcanism and seismicity.

After merging the three maps, T_e blends the large-scale features of the 800x800 km window with the finer details observed in the smaller windows (Figures 6 and 7). Some of the key features observed in the merged results include corridors of relatively low T_e connecting the Hoggar, Tibesti and Darfur hotspots and a corridor connecting the latter to local T_e minima in the western Ethiopian plateau to the east and to the Cameroon volcanic line to the west.

10

Relatively low T_e connects the western branch of the East Africa rift to the western Ethiopian plateau, the Afar constitutes a global T_e minimum, and southeast of Lake Turkana there is a marked local T_e minimum. Westward, relatively low T_e appears to encroach toward the centre of the Tanzania craton (east of Lake Victoria). Further to the southwest, a NE-SW low T_e lineament that follows the border of the Congo craton and coincides with the Meso-Proterozoic Kibaran belt has low T_e and prominent seismic activity (Figures 6b and 7c). The Kalahari craton exhibits some T_e variation within its interior, with relatively low T_e around the 2.1 Ga Bushveld magmatic complex.

_____

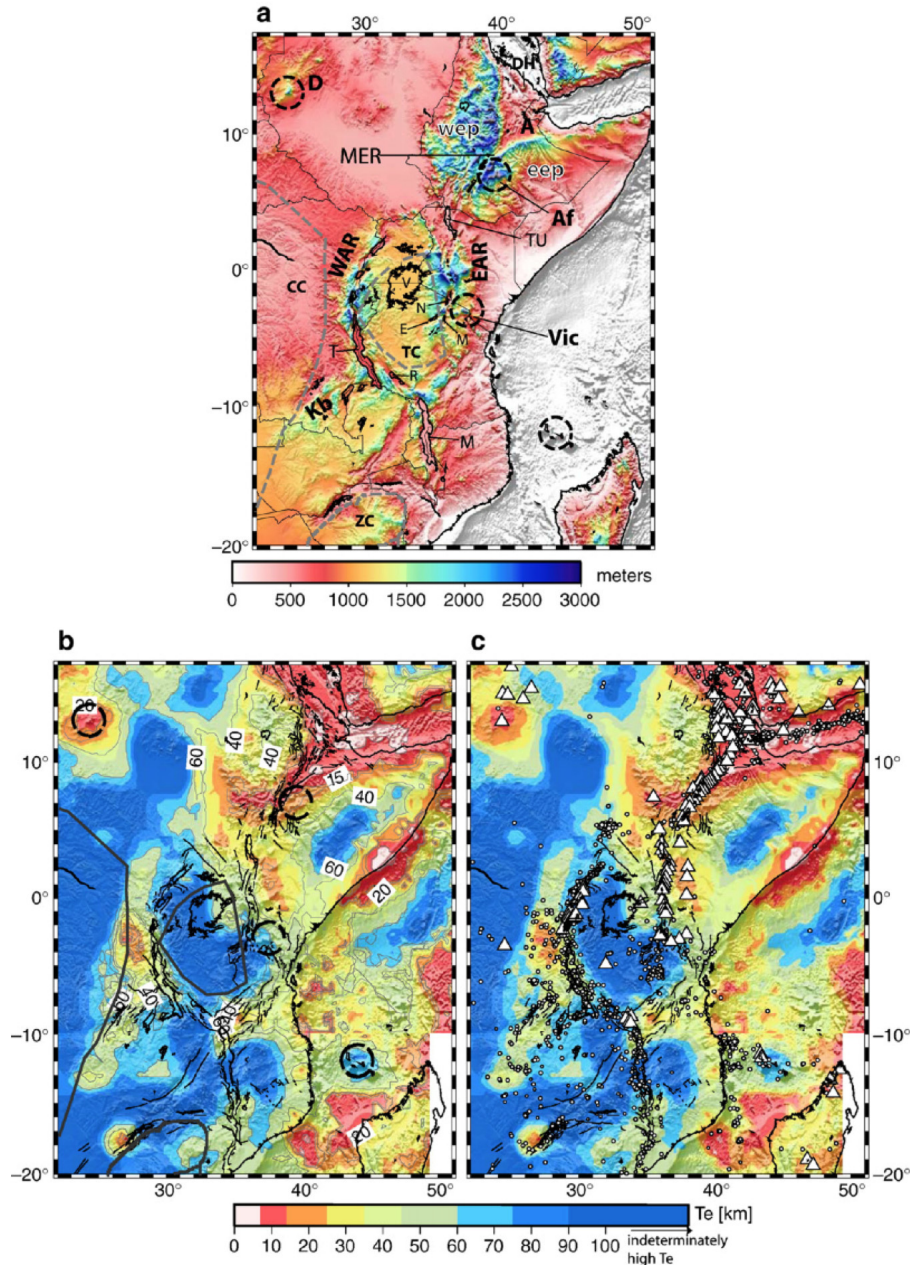**Figure 7. a)** Topography of East African rift system with delineation of cratons and proposed location for hot-spots superimposed. CC: Congo craton, TC: Tanzania craton, ZC: Zimbawe craton. A: Afar, MER: Main Ethiopian rift, wep: western Ethiopian plateau, eep: eastern Ethiopian plateau, WAR: western branch of the East African rift, EAR: eastern branch of the East African rift. R: Lake Rukwa, T: Lake Tanganika, M: lake Malawi, V: lake Victoria. N: lake Natron, E: lake Eyasi, M: Lake Manyara, TU: Lake Turkana. Vic and Af are proposed location for Victoria and Afar hotspots, respectively. **b)** Close up of T_e results shown in Figure 6 with main active faults and cratons superimposed. **c)** Same as in b) but overlain by Cenozoic volcanoes and earthquakes with magnitude $M_b > 4.5$.

In the ocean basins, T_e primarily represents the strength of the lithosphere at the time of loading. Where there has been neither volcanism nor sedimentation since the lithosphere was first created, T_e represents the strength at the time of oceanic crust formation (and hence is very low). In some hotspots such as the Canaries, T_e is higher than that estimated from the basement deflection around these volcanic islands. This likely reflects differences between the CRUST2.0 density structure input to our model and the actual crustal structure in these small islands. In the following we discuss our results within continental Africa in detail.

6. Discussion

6.1. Comparison with previous studies of T_e in Africa

The paucity of uniform continental-scale gravity anomaly data coverage in Africa has limited the number of continental-scale T_e studies. Exceptions are those by Hartley et al. (1996) and Mantovani et al. (2005). Hartley et al. (1996) used the Bouguer coherence from periodogram spectra to estimate T_e. The data incorporated no satellite measurements and the terrestrial measurements were much sparser than in the EGM2008 gravity model used here. As a consequence, Hartley et al. (1996) measured the coherence at randomly distributed locations using variable window sizes, instead of the 50 km spacing for T_e calculation that has been used here. Nonetheless, Hartley et al. (1996) also found high T_e over the West African, Congo, Tanzania and Kalahari cratons, and low T_e over the Afar and East African rifts, but the detailed variation of T_e is different from our results. We attribute this to the paucity of their data, to the fact that their T_e is estimated at much fewer and at unevenly distributed locations, and to their use of a more rudimentary periodogram spectral estimator having unknown (and hence uncorrected) estimate bias.

Mantovani et al. (2005) estimated T_e using an empirical correlation between tidal gravity anomalies and elastic thickness, and used this correlation to generate elastic thickness estimates where terrestrial gravity measurements were sparse. They found high T_e over the West African and Congo cratons and also on parts of the Kalahari. They also found lower T_e over the East African and Ethiopian rifts and over the Cameroon volcanic lines. However, the wavelength of the variation of their T_e values is much larger than ours, and so a comparison is also difficult. The long wavelength of their results may be due to the very few African T_e measurements that they used for their correlation.

The effective elastic thickness also was estimated in South Africa using the coherence function by Doucouré et al. (1996). These authors used variable window sizes and a periodogram spectral estimator, and they did not correct for bias due to windowing. They estimated T_e in only 4 windows, finding relatively low T_e over the Namaqua belt surrounding the Kapvaal craton (T_e of 38 km to 48 km) and high T_e in a window centred in the Kapvaal craton. These results are not contradictory to ours, which are computed every 50 km and take into account windowing effects, and show a relatively strong Kapvaal craton with some low T_e areas within it. Stark et al. (2003) calculated T_e in South Africa using a wavelet based coherence function. The spatial variations of T_e in their study are much smoother than in ours (T_e ranges from 25 to 80 km in their study). Pérez-Gussinyé et al. (2009) examine comprehensively T_e estimates based on wavelets and windowing approaches. Based on their results we believe that the T_e estimates of Stark et al. (2003) represent a smoothed version of ours, in the same manner that the wavelet based T_e of South America was a smoothed version of the multitapered estimates (Pérez-Gussinyé et al., 2009).

Our T_e map agrees generally well with previous studies of T_e in the East African and Ethiopian rifts. The general pattern of high T_e (>60 km) over the Tanzania craton surrounded by lower T_e underlying both branches of the East African rift and a T_e minima over the Afar triangle has been demonstrated in previous studies (Ebinger et al., 1989; Petit and Ebinger, 2000; Tessema and Antoine, 2003). Direct comparison of absolute T_e and detailed variation in T_e is problematic however. Some of the earlier T_e analyses were performed along single profiles, and a quantitative comparison would have little meaning. Most of the coherence studies used periodogram spectral estimation, estimated T_e using windows whose centres where not regularly spaced, and merged results obtained from windows of different sizes without correcting for windowing bias. Despite this, previous authors have used large windows to estimate T_e over cratonic areas, such as the Tanzania craton, and small windows to estimate T_e over areas undergoing large amounts of extension, as Afar, so that the overall pattern of T_e variations is similar. New features that our analysis reveals include relatively low T_e in the western Ethiopian plateau, a local T_e minimum located southeast of Lake Turkana, and relatively low T_e encroaching into the centre of the Tanzania craton (east of Lake Victoria). Effective elastic thickness was also estimated in West Africa by Poudjom Djomani et al. (1995) using periodogram coherence, obtaining a similar pattern of variation to ours with a T_e minimum over the Cameroon Volcanic Line. In the following subsections we discuss new features revealed by our analysis and examine how they relate to other proxies for lithospheric thickness and to surface tectonics.

6.2 Large cratonic areas

Cratonic areas are commonly associated with high T_e (>60 km, Ebinger et al., 1989; Pérez-Gussinyé and Watts, 2005). This high T_e is consistent with the low heat-flow and fast seismic velocities measured at great depth in cratonic areas. In Africa too, effective elastic thickness is highest in the West African, Congo, Tanzania and Kalahari cratons (Figure 6). In general, lower T_e is found in the Kalahari than in other cratons. Also, while the Congo and West African cratons are characterized by negative Bouguer anomalies of ~0 to –100 mGals and subdued topography, the Tanzania and Kalahari cratons are characterized by much more negative Bouguer anomalies, < -150 mGals, and high plateaus. As the crust is not obviously over-thickened in the latter cratons, the very negative Bouguer anomalies may indicate atypically buoyant lithospheric or asthenospheric mantle supporting the high topographic elevations.

Within the Kaapval there are local T_e minima centred southwest of the western limb of the Bushveld magmatic province, on the eastern limb of the Bushveld magmatic province (Figure 6 and Figure 1 for location). Thus, the Kapvaal does not seem to be a uniformly rigid craton. In accordance, Griffin et al. (2003) find strong lateral heterogeneity in the composition of the lithospheric mantle beneath the Kapvaal and relate it to modification of the original Archean mantle by metasomatism during the Phanerozoic.

Our T_e estimates in the Kapvaal, which are lower than in other African cratons, may point to an originally rigid Kapvaal cratonic lithosphere that has been weakened by heating and metasomatism, probably related to the greatest concentration of hotspots beneath Africa during the Phanerozoic, such as the Karoo, Tristan da Cunha, Kerguelen and Reunion, as shown by Morgan (1983). Whether the earlier asthenospheric thermal anomaly still exists is a matter of much debate, as is the question of whether heating has thinned the original thick cratonic lithosphere. While many analyses of xenoliths in South Africa agree on an original cratonic mantle modified by later magmatic events (Bell et al., 2003; Griffin et al., 2003),

seismic tomography studies differ in their estimates of lithosphere thickness and its lateral variations within the craton.

Priestley and Tilman (2009) argue that the differences between seismic images stem from the different depth and lateral resolutions that body and surface waves provide. While body wave tomography studies finds a high velocity lid up to 300-400 km beneath South Africa, which is thinner beneath the Bushveld (James et al., 2001; Fouch et al. 2004), surface wave tomography studies, including fundamental and higher order modes, suggest a laterally uniform lid thickness of 180 ± 20 km (Li and Burke, 2006) and up to 170-200 km (Priestley et al., 2008; Priestley and Tilmann, 2009). Priestley and Tilmann (2009) show with synthetic data that the high velocity lid extending to a depth of ~400 km observed with body waves is an artefact due to poor vertical resolution of body wave tomography. Additionally their surface wave tomography shows smaller lithospheric lid thickness in the Kapvaal (170-200 km) than in the other African cratons (225-250 km), consistent with lower T_e there than in other cratons. Priestley and Tilmann (2009) and Li and Burke (2006) also find a low velocity zone beneath the South African lithosphere. Likewise, Wang et al. (2008) use joint modelling of seismic and mineral physics data to find a low velocity zone with large velocity reductions beneath a ~150 km lithospheric lid, which they relate to either a high temperature gradient or the presence of partial melt, both of which could explain the observed localized uplift in the African Superswell. Thus, lower T_e observed beneath the Kalahari relative to other cratons is at least consistent with the seismic observations.

6.3. East African and Ethiopian rifts

The strength of the lithosphere, and hence T_e, decreases with the increase in geothermal gradient that results from heat advection due to both extension and to melt transport (Ebinger, et al. 1999; Buck, 2004). Within the Ethiopian and East African rifts, we estimate lower T_e where seismic lithospheric lids are thin and where low seismic velocities have been imaged at asthenospheric depths. Low seismic velocities (particularly low S velocities) may indicate a thermal anomaly with concomitant increase of geothermal gradient and lower T_e. Here, we describe our results and relate them to variations in seismic lid thickness and/or the existence of seismic velocity anomalies beneath the lithosphere. We also discuss how T_e relates to varying seismogenic layer thicknesses and rift segmentation styles.

The lowest T_e in the continent occurs in the Afar region, followed by the Main Ethiopian rift (MER, Figure 6). A close up of this region (Figure 7) shows T_e minima (<7 km) along the inland propagation of the Gulf of Aden and the postulated inland propagation of the southern Red Sea, west of the Danakil block, where extension is maximum (Wolfenden et al., 2004).

T_e in the rest of MER and Afar is < 15 km (Figure 7). A striking feature of the MER is that the deformation zone between both rift shoulders is very narrow and this coincides with T_e < 15 km. Within the rift valley, deformation is further concentrated in a narrow (< 20 km wide) zone where extensional strain and magmatism focuses along short fissures, faults and en-echelon magmatic segments aligned in volcanic cones (Bilham et al., 1999; Ebinger and Casey, 2001; Keir et al. 2006). T_e increases sharply on both shoulders of the rift, but is much higher on the Eastern plateau than on the Western Ethiopia plateau, as we will discuss later. Following Ebinger (2005) we expect that the original segmentation of the MER was similar to that of the Tanzania rift, where the development of the rift in a strong lithosphere has resulted in few long faults (>100 km) which border relatively wide half-grabens. In the MER these older border faults control the location of the main rift valley (Ebinger, 2005).

Increasing extension and accompanying magmatism focuses within the rift valley, leading to weakening and further focusing of deformation where magmatism occurs. Both focused deformation and magmatism led to the low T_e observed today, which in turn led to the development of short rift segments within the MER. Hence, the present configuration of the MER is probably the result of rifting strong lithosphere and subsequent lithospheric weakening due to extension and magmatism, which led to further narrowing of the zone of deformation. A weak lithosphere at the onset of rifting, such as that proposed for the Basin and Range, would have favored the development of wide rifting accommodated by many extensional grabens (Buck, 1991).

On both rift shoulders of the MER and Afar, T_e increases. This is in accordance with receiver function estimates of lithosphere thickness that suggest a thicker seismic lid, ~70-80 km, beneath the western Ethiopian plateau than beneath the Afar and MER, where it is estimated to be ~50 km thick (Dudga et al., 2007). The thin lithospheric mantle in the MER and Afar likely has negligible strength, and the T_e of ≤15 km mainly reflects the strength of the upper elastic crust, as earthquakes are mainly concentrated ~10 to 14 km and occur to a depth of 18 km (Keir et al., 2006).

West of the MER, on the western Ethiopian Plateau, there is a marked relative low in T_e (< 20 km) between latitudes 5° to ~10° N (Figures 6 and 7). Tomographic images reveal a ~500 km wide area with low P and S wave velocities from 75 to ≥400 km depth in the upper mantle that extends from close to the eastern edge of the Main Ethiopian Rift (MER) westward beneath the uplifted and flood basalt-capped western Ethiopian Plateau (Bastow et al., 2008). The center of this low velocity anomaly coincides with the center of our low T_e zone in the western plateau. The low seismic velocities are attributed to the presence of a thermal anomaly and melt at asthenospheric levels (Bastow et al., 2008). Bastow et al. (2008) suggest that this low seismic velocity zone is connected to a low seismic velocity anomaly in the lower mantle beneath South Africa and provides the main melt volume that later feeds into the MER and Afar. Low T_e in this region probably relates to advective heating by melt intrusions into the lithosphere interpreted from shear wave splitting studies (Kendall et al., 2005), and to the thin seismic lid, ~70-80 km, which likely reflects thermal erosion of the lithosphere by the underlying hot mantle (see Dudga et al., 2007 for a discussion on this topic). Magnetotelluric studies also show that the lower crust under the eastern Ethiopia plateau is more resistive than under the western plateau (Whaler and Hautot, 2006), consistent with interpretations of intrusions and a lower T_e under the western than under the eastern plateau (Figure 7).

Southwards from the Ethiopian Plateau, relatively low T_e (< 30 km) continues along Lake Turkana and to the southeast, where the pattern of volcanism follows two parallel main trends (Figures 6 and 7). This area of relatively low T_e extends along the Kenyan rift valley, but its minimum is centered to the east in an off-rift location at ~38°E, 1°N, where there is volcanism but no seismicity (Figure 7). This relative minimum in T_e occurs at the northern tip of the location proposed by some authors for the Victoria hotspot (Morgan and Phipps Morgan, 2006; Montagner et al., 2007; Figures 6 and 7). We suggest that low T_e in the Kenya rift, where there is volcanism and seismicity, is due to tectonic lithospheric thinning and further weakening by magmatic processes. In the off-rift T_e minima location, weakening is probably only due to thermal and magmatic processes, as seismicity there is (currently) absent. It is worth noting that T_e in the Kenya rift is higher than that in the MER and Afar, where lithospheric thinning and magmatism are more pronounced. Thus, as expected, T_e decreases with the amount of extension.

The T_e structure in the Tanzania craton appears more complex than found in previous studies (Ebinger et al., 1989; Tessema and Antoine, 2003). Instead of a single and homogeneous high rigidity block occupying the whole craton, we observe a clear decrease of the elastic thickness affecting the northeastern part of the craton towards the east of Lake Victoria (Figures 6 and 7). The reduced T_e is observed in all three data window sizes (Figure 5) but is clearest with the small window size (Figure 5c). This behaviour is consistent with simulations of T_e recovery from a small T_e area embedded in a large T_e area (Pérez-Gussinyé et al., 2009). Thus we believe this low T_e anomaly is real. This T_e minimum coincides with a relative minimum in Bouguer anomaly and a relative maximum in topography east of Lake Victoria (Figure 1). The differences between previous T_e studies (Ebinger et al. 1989; Tessema and Antoine, 2003) and our results probably stem from the more complete EGM2008 data set used here, from methodological differences (the use of merged and bias-corrected T_e values and a multitaper instead of periodogram spectral estimation), and from much finer window sampling in this study. The relative low T_e coincides with the location of a radial seismic anisotropy that, according to Weertrane et al. (2003), corresponds to the centre of a head plume beneath the Tanzania craton. Low T_e may arise from modification of the lithospheric mantle by an underlying hot mantle either by the more inefficient process of heat conduction or by heat advected by melts intruded into the lithosphere. Which of the processes dominates depends on the unknown amount of intruded melt, but the ~ 100 Myr timescale required for thermal conduction through a thick, cold lithosphere would suggest advection plays a role.

The eastern part of the Tanzanian craton terminates ~3-2°S near the latitude of Lake Natron (Figure 7). Thus along the eastern rift branch T_e increases southward as the rifts widens from a 50 km rift zone in southern Kenya to a > 200 km zone in the northern Tanzania divergence (Figure 7) and earthquake hypocentral depths increase (Albaric et al., 2008), consistent with the observed increase in T_e. Structural and metamorphic studies in the eastern rift branch (Smith and Mosley, 1993) suggest that the transition from thin mobile belt lithosphere to Archean lithosphere occurs near the latitude of Lake Natron, coincident with our results (Figure 7). It is difficult to understand however why the eastern rift branch is propagating south along Lake Natron, Eyasi and Manyara (as suggested by geodetic observations, Calais et al., 2008) where the lithosphere is thick and rigid, instead of propagating through the zone of low T_e found east of Lake Victoria (Figure 7). This suggests that extension does not always follow pre-existing weaknesses. Calais et al. (2008) observed a magmatic dyking event and associated seismicity and suggest that the buoyancy provided by magma and the reduction in plate strength due to magmatic heating may play significant roles in localizing extension in rigid cratonic lithospheres. Thus lateral variations in large-scale strength of the lithosphere may not be the only factor controlling deformation, if melt percolation pathways can determine the locus of new extensional events.

The western branch of the East African rift has its lowest T_e along the northern half of Lake Tanganyika and westwards from it, where seismicity clusters (Figure 7). Northwards and southwards from this area, T_e increases and it only decreases locally over Lakes Rukwa and Malawi. This decrease of T_e is only observed with the smallest analysis windows and is partially smoothed in the merged T_e results (compare Figure 5c and Figure 7). The broad zone of low T_e at the border between Mozambique and Tanzania (Figure 7) coincides with an area of active extension, but at slow rates (Stamps et al., 2008).

A NE-SW lineament of low T_e follows the border of the Congo craton and coincides with the Meso-Proterozoic Kibaran belt, which has prominent seismicity (Figures 6b and 7). This low

T_e zone correlates with active faulting and may mark a direction of propagation of the EAR system.

6.4 Hot-spots in central and western Africa

The West and Central African rifts systems (WARS and CARS in Figure 1) are Mesozoic structures formed due to stress build-up in response to the differential opening of the South and Central Atlantic oceans (Guiraud and Maurin, 1992). The majority of the present volcanism within western and central Africa does not, however, lie in the location of Mesozoic rifts, with the exception of the Cameroon volcanic line, which lies in the Mesozoic Benue trough of Nigeria (Guiraud and Maurin, 1992; Figure 6). The causes of the Tertiary-Quaternary volcanism in western and central Africa are not understood. Based on geochronological data and numerical modelling, Ebinger and Sleep (1998) suggested that the spreading of a ~45 Ma old plume centred beneath Afar could explain much of the intra-continental volcanism, such as Darfur and the Cameroon line. Alternatively, it has been suggested that intra-continental hotspots beneath Africa represent small-scale convective instabilities arising at the sharp transitions between very thick cratonic lithosphere in the Congo and West African cratons and zones of pre-existing thinned lithosphere (Montagner et al., 2006; King and Ritsema, 2000). Whatever the mechanisms for the Hoggar, Tibesti, Darfur and Cameroon line, geochemical and seismic observations strongly suggest that their source is shallower than that of the Afar hotspot (King and Ritsema, 1999; Montagner et al., 2007; Sebai et al., 2006; Priestley et al., 2008). Our results show that the Hoggar, Tibesti, Darfur and Cameroon line hot-spots collocate with low elastic thickness bounded by high elastic thickness corresponding to the Congo craton to the south, the West African craton to the west and the Unweinat inlier to the east. Brown and Girdler (1980) interpreted the negative Bouguer gravity anomalies in the Darfur, Hoggar and Tibesti to be produced by a low density root at depth caused by lithospheric thinning through the replacement of lithosphere by hotter, lower density asthenosphere. Crough (1981a, b) calculated the depth of this root, and found values of ~60 km for the Hoggar and 40-80 for Darfur. Thus, the relatively thin, hot lithospheres over these areas are consistent with the low T_e estimated here.

Our results show that the Hoggar, Tibesti and Darfur are connected to each other by narrow corridors of relatively low T_e lithosphere (Figure 6). The Darfur hot-spot is also connected by low T_e corridors to the Cameroon line, and to the low T_e area in the western Ethiopian plateau which is underlain by a low P and S seismic anomaly which extends at least to 400 km depth (Bastow et al., 2008). The NW-SE low T_e corridor connecting the western Ethiopian plateau to the Hoggar, Tibesti, and Darfur is an extensive fault zone which today shows neither seismic nor volcanic activity and is interpreted by Guiraud et al. (2000) to have been re-activated at various times during the Phanerozoic. We suggest that the relative low T_e in these corridors (60-80 km) indicate that the lithosphere along them is thinner than in the surrounding cratonic regions. We speculate that pre-existing thin lithosphere locally enabled hot asthenospheric material, with a source near the western Ethiopian plateau, to rise to sufficiently shallow depths (<90 km) to generate partial melts under volcanic provinces of central and western Africa, as suggested by Ebinger and Sleep (1998).

7. Conclusions

We have generated a new map of T_e of Africa using the most up-to-date gravity anomaly database available. The map derives from a new approach to Bouguer coherence analysis in which we optimally combine estimates from several differently-sized data windows and correct for bias error terms calculated via simulations of T_e recovery from synthetic data. We

To be published in Earth and Planetary Science Letters
Earth Planet. Sci. Lett., 287(1-2), 152-167, 2009

find that, in general, high T_e coincides with thick seismic lithospheric lids. Areas of low T_e coincide with thinner seismic lids and sometimes with the existence of deep seismic anomalies at sub-lithospheric depths. Our results correspond well with previous T_e estimates in the continent but have an improved lateral resolution, mainly due to the more modern database and estimation techniques. The large-scale pattern of T_e variations consist of high T_e over cratons, and low T_e over the Ethiopian and East African rift and the volcanic provinces of intra-continental Africa.

Our T_e variations delineate with high lateral accuracy the areas of lowest T_e in Africa, which coincide with the narrow Main Ethiopian rift and the Afar triangle, where lithospheric extension is greatest and seismic lids are thinnest. Within the Afar triangle the absolute minima are located along the inland propagation of the Aden rift, in Djibouti, and the inland propagation of the Red Sea rift, west of the Danakil horst.

New features that our images reveal consist of relatively lower T_e over the Kalahari craton than in other cratons, relative low T_e within the western part of the Ethiopian plateau, relative low T_e on the northeastern side of the Tanzania craton just east of Lake Victoria, and relative low T_e over the intra-continental volcanic provinces of Tibesti, Darfur, Hoggar and Cameroon lines. Corridors of relatively low T_e connect these provinces to each other and to the low T_e area on the western Ethiopia plateau.

We interpret that the relatively low T_e found in the Kalahari and Tanzania cratons result from modification of cratonic lithosphere by sub-lithospheric thermal anomalies. In the case of the Kalahari craton, surface wave tomography and combined modelling of seismic and mineral physics data suggests the presence of an anomalously hot asthenospheric mantle. In the Tanzania craton, our low T_e anomaly is located over the centre of radial seismic anisotropy below the craton, interpreted in previous works as the head of the Victoria plume.

The relative T_e minimum over the western Ethiopian plateau is located above a region of low P and S seismic velocities extending to at least 400 km depth that has been interpreted by other authors as the head of the Afar plume. Low T_e in this area is probably related to weakening by heat advected by magmatism. This area is connected by corridors of low T_e to Tibesti, Darfur, Hoggar and Cameroon line intra-continental volcanic provinces, which themselves have low T_e. The low T_e corridors connecting the western Ethiopian plateau to the Tibesti, Darfur, Hoggar run over an area of extensive Phanerozoic faulting, which today shows neither seismic nor volcanic activity. We interpret that the low T_e indicates that the lithosphere in those corridors is thinner than in the surrounding cratonic areas. Thus, we speculate that these low T_e corridors may provide potential conduits for hot asthenospheric material to flow from the western Ethiopian plateau, which is underlain by a deep-seated seismic anomaly to the rest of volcanic provinces of central and western Africa, where no deep seismic anomalies have been observed.

References
[1] Albaric, J., J. Deverchere, C. Petit, J. Perrot, B. Le Gall, 2009. Crustal rheology and depth distribution of earthquakes: Insights from the central and southern African rift systems, *Tectonophysics*, in press.
[2] Bastow, I. D., G.W. Stuart, J-M Kendall, C. Ebinger, 2005. Upper-mantle seismic structure in a region of incipient continental break-up: northern Ethiopia, Geophys. J. Int., 2005, 162, 479-493.

[3] Bastow, I. D., Nyblade, A. A., Stuart, G. W., Rooney, T. O., Benoit, M.H., 2008. Upper mantle seismic structure beneath the Ethiopian hot spot: Rifting at the edge of the African low velocity anomaly, G-cubed, 9, doi:10.1029/2008GC002107.

[4] Bell, D. R., Scmitz, D. R., Janney, P. E., Mesozoic thermal evolution of the southern African mantle lithosphere, Lithos, 71, 273-287, 2003.

[5] Benoit, H., A.A. Nyblade, J. C. VanDecar, Upper mantle P-wave speed variations beneath Ethiopia and the origin of the Afar hotspot, Geology, 2006, 34, 329-332, doi:10.1130/G22281.1.

[5] Bilham, R., Bendick, R., Larson, K., Mohr, P., Braun, J., Tesfaye, S., Asfaw, L., 1999. Secular and tidal strain across the main Ethiopian rift, J. Geophys. Res., 26, 2789-2792.

[6] Brown, C. D., Phillips, R. J., 2000. Crust-mantle decoupling by flexure of continental lithosphere, J. Geophys. Res., 105, 13,221–13,238.

[7] Brown, C. Girdler, R.W., 1980, Interpretation of African Gravity and its implications for breakup of continents, J. Geophys. Res., 85, 6443-6455, 1980.

[8] Buck, W. (1991), Modes of Continental Lithospheric Extension, J. Geophys. Res., 96(B12), 20161-20178.

[9] Buck W R 2004 in Karner G *et al.* (eds) Rheology and deformation of the lithosphere at continental margins, (Columbia Univ. Press) 92–137.

[10] Burke, K., The African plate, S. Afr. Plate, S. Afr. J. geol. 99, 339-410, 1996.

[11] Burov, E., Diament, M., 1995. The effective elastic thickness (Te) of continental lithosphere: What does it really mean?, J. Geophys. Res., 100, 3905– 3927.

[12] Calais, E., N. d'Oreye, J. Albaric, A. Deschamps, D. Delvaux, J. Deverchere, C. Ebinger, R. W. Ferdinand, F. Kervyn, A. S. Macheyeki, A. Oyen, J. Perrot, E. Saria, B. Smets, D. S. Stamps, C. Wauthier, 2008, Aseismic strain accommodation by slow slip and dyking in a youthful continental rift, East Africa, Nature, Vol 456, doi:10.1038/nature07478.

[13] Crough, S.T., 1981a. The Darfur swell: gravity constraints and its isostatic compensation, Geophys. Res. Lett., 8, 877-879.

[14] Crough, S.T., 1981b, Free-air gravity over the Hoggar massif, northwest Africa: evidence for lateration of the lithosphere, Tectonophysics, 77, 189-202.

[15] Doucouré, C. M., de Wit, M.J., 1996, Effective Elastic thickness of the continental lithosphere in South Africa, J. Geophys. Res., 101, 11,291-11,303.

[16] Dudga, M.T., Nyblade, A.A., Julia, J., 2007. Thin lithosphere beneath the Ethiopian plateau revealed by a joint inversion of Rayleigh wave group velocities and receiver functions, J. Geophys. Res., 112, doi:10.1029/2006JB004918.

[17] Eaton, D. W., Darbyshire, F., Evans, R.L., Grüter, H., Jones, A.G., Yuan, X., The elusive lithosphere-asthenosphere boundary (LAB) beneath cratons, in press, Lithos.

[17] Ebinger, C. J., T.D. Bechtel, D. W. Forsyth and C. O. Bowin, 1989, Effective Elastic Thickness beneath the East African and Afar Plateaus and Dynamic compensation for the uplifts, *J. Geophys. Res.*, 94, 2883-2901.

[18] Ebinger, C. J., Y. Poudjom Djomani, E. Mbede, A. Foster and J.B. Dawson, 1997. Rifting Archean lithosphere: The Eyasi-Manyara-Natron rifts, East Africa, J. Geol. Soc., 154, 947-960.

[19] Ebinger, C. J., Sleep, N. H., 1998. Cenozoic magmatism throughout east Africa resulting from impact of a single plume, Nature, 395, 788-791.

[20] Ebinger, C.J., Jackson, J.A., Foster, A. N., Hayward, N.J., 1999, Extensional basin geometry and the elastic lithosphere, *Phil. Trans. R. Soc. Lond.,* 357, 741-765.

[21] Ebinger, C., Casey, M., 2001. Continental breakup in magmatic provinces: An Ethiopian example, Geology, 29, 527-530.

[22] Ebinger, C.J., 2005. Continental break-up: The East African perspective, *Astronomy & Geophysics*, Volume 46, Issue 2, pp. 2.16-2.21.

[23] Fernàndez, M., Afonso, J.C. and G. Ranalli. 2009. The deep lithospheric structure of the

Namibian volcanic margin, Tectonophysics, doi:10.1016/j.tecto.2009.02.036

[24] Finnerty, A.A. and F.R. Boyd, 1987, Thermobarometry for garnet peridotites: basis for the determination of thermal and compositional structure of the upper mantle. In: Nixon, P.H. (Ed.), Mantle Xenoliths, Wiley & Sons, pp. 381-402.

[25] Forsyth, D. W. (1985), Subsurface loading estimates of the flexural rigidity of continental lithosphere, J. Geophys. Res., 90, 12,623– 12,632.

[26] Fouch, M.J., James, D.E., VanDecar, J.C., van der Lee, S., and Kapvaal Seismic Group, 2004. Mantle seismic structure beneath the Kaapvaal and Zimbawe cratons, S. Afr. J. Geol., 107, 33-44.

[27] Fullea, J., M. Fernàndez, and H. Zeyen (2008), FA2BOUG-a FORTRAN 90 code to compute Bouguer gravity anomalies from gridded free air anomalies: application to the Atlantic-Mediterranean transition zone, *Computers & Geosciences*, 34, 1665-1681.

[28] Fullea, J., M. Fernàndez, H. Zeyen, and J. Vergés (2007), A rapid method to map the crustal and lithospheric thickness using elevation, geoid anomaly and thermal analysis. Application to the Gibraltar Arc System and adjacent zones, *Tectonophysics*, 430, 97-117.

[29] Griffin, W.L., S. O'Reilly, L.M. Natapov and C.G. Ryan, The evolution of lithospheric mantle beneath the Kalahari Craton and its margins, Lithos, 71, 215-241, 2003.

[30] Guiraud, R., Maurin, J.-C., 1992. Early Cretaceous rifts of western and central Africa: an overview, *Tectonophys.*, 213, 153-168.

[31] Guiraud, R., Doumnang Mbaigane, J.-C., , Carretier, S., Dominguez, S., 2000. Evidence for a 6000 km length NW-SE-striking lineament in northern Africa: The Tibesti lineament, Journal of the Geological Society, London, 157, 897-900.

[32] Hartley, R., Watts, A.B., Fairhead, J.D., 1996. Isostasy of Africa, *Earth and Planet. Sci. Lett.*, *137*, 1-18.

[33] Hofmann, C., Courtillot, V., Féraud, G., Rochette, P., Yirgu, G., Ketefo, E., Pik, R., 1997. Timing of the Ethiopian flood basalt event and implications for plume birth and global change, Nature, 398, 838-841.

[34] Kendall, J.-M., Stuart, G. W., Ebinger, C.J., Bastow, I.D., Keir, D., 2005. Magma-assisted rifting in Ethiopia, Nature, vol. 433, 146-148.

[35] James, D.E., Fouch, M. J., VanDecar, J. C., van der Lee, S. and the Kaapvaal Seismic Group, 2001, Tectospheric structure beneath South Africa, Geophys. Res. Lett., 28, 2485-2488.

[36] Jones, A.G., 1999. Imaging the continental upper mantle using electromagnetic methods, Lithos, 48, 57-80.

[37] Jordan, T. A., Watts, A. B., 2005. Gravity anomalies, flexure and the elastic thickness structure of the India-Eurasia collisional system, Earth Planet. Sci. Letts., 236, 732-750.

[38] Keir, D. Ebinger, C.J., Stuart, G. W., Daly, E., Ayele, A., 2006, Strain accommodation by magmatism and faulting as rifting proceeds to break-up: Seismicity of the northern Ethiopian rift, J. Geophys. Res., 111, B05314, doi:10.1029/2005JB003748.

[39] King, S. D. and J. Ritsema, 2000. African hotspot volcanism: small-scale convection in the upper mantle beneath cratons, Science, 290, 1137-1140.

[40] Kirby, J.F., C. J. Swain, 2008. An accuracy assessment of the fan wavelet method for elastic thickness estimation, *G-cubed, 9*, Q03022, doi:10.1029/2007GC001773.

[41] Laske, G., Masters, G. & Reif, C. The Reference Earth Model Website. http://mahi.ucsd.edu/Gabi/rem.html (2000).

[42] Li, A., Burke, K., 2006. Upper mantle structure of southern Africa from Rayleigh wave tomography, J. Geophys. Res, doi:10.1029/2006JB004321.

[43] Lithgow-Bertelloni, C., Silver, P.G., 1998. Dynamic topography, plate driving forces and the African Superswell, *Nature*, *395*, 269-272.

[44] Lowry, A. R., Smith, R. B. 1995. Strength and rheology of the western U.S. Cordillera, J. Geophys. Res., 100, 17,947– 17,963.

[45] Lowry, A.R., Ribe, N.M., Smith, R.B., 2000. Dynamic elevation of the Cordillera, western United States, J. Geophys. Res., 105, 23,371-23,390.

[46] Mareschal, J.C., Jaupart, C., 2004. Variations of surface heat flow and lithospheric thermal structure beneath the North American craton, Earth and Planetary Science Letters, 223(1-2), 65-77, doi: 10.1016/j.

[47] Mantovani, M., Shukowsky, W., Freitas, S.R.C., Brito Neves, B. B., 2005. Lithosphere mechanical behavior inferred from tidal gravity anomalies: a comparison of Africa and South America, Earth Planet. Sci. Lett., 397-412.

[48] Menzies, M. A. et al., Integration of geology, geophysics and geochemistry: A key to understanding the North China Craton, Lithos, 96, 1-21, 2007.

[49] Montagner, J.P., B. Marty, E. Stutzmann, D. Sicilia, M. Cara, R. Pik, J-J., Leveque, G. Roult, E. Beucler, E. Debayle, 2007. Mantle upwellings and convective instabilities revealed by seismic tomography and helium isotope geochemistry beneath eastern Africa. Geophys. Res. Lett., doi:19.1029/2007GL031098.

[50] Morgan, W.J., 1983, Hotspot tracks and early rifting of the Atlantic, Tectonophysics,123- 139.

[51] Morgan, W.J., Phipps Morgan, J., 2007. Plate velocities in the hotspot reference frame, in Foulger G.R. and Jurdy, D.M., eds. Plates, plumes and planetary processes: Geological Society of America Special Paper 430, 65-78, doi:10.1130/2007.2430(04).

[52] Nürnberg, D., Müller, R.D., 1991. The tectonic evolution of the South Atlantic from Late Jurassic to present. Tectonophysics, 191: 27-53.

[53] Nyblade, A.A. and S. W. Robinson, 1994. The African superswell, Geophys, Res. Lett., 21, 765-768.

[54] Pavlis, N., S. Holmes, S. Kenyon, J. Factor, An Earth Gravitational Model to Degree 2160: EGM2008, EGU General Assembly, Vienna, Austria, 2008.

[55] Pérez-Gussinyé, M., Lowry, A. R., Watts, A. B., Velicogna, I., 2004. On the recovery of the effective elastic thickness using spectral methods: examples from synthetic data and from the Fennoscandian Shield, *J. Geophys. Res., 109*, doi: 10.1029/2003JB002788.

[56] Pérez-Gussinyé, M., Watts, A.B., 2005, The long-term strength of Europe and its implications for plate forming processes, Nature, 436, 381–384, doi:10.1038/nature03854.

[57] Pérez-Gussinyé, M., Swain, C. J., Kirby, J.F., Lowry, A. R., Spatial variations of the effective elastic thickness, T_e, using multitaper spectral estimation and wavelet methods: examples from synthetic data and application to South America, in press in G-cubed.

[58] Petit, C., Ebinger, C., Flexure and mechanical behavior of cratonic lithosphere: Gravity models of the East African and Baikal rifts, J. Geophys. Res., 19,151-19,162, 2000.

[59] Poudjom-Djomani, Y.H., Nnange, J.M., Diament, M., Ebinger, C.J., Fairhead, J.D., 1995. Effective elastic thickness variations in west central Africa inferred from gravity data, J. Geophys. Res., 100, 22,047-22,070.

[60] Priestley and Tilmann, Relationship between the upper mantle high velocity seismic lid and the continental lithosphere, 2009, Lithos, 109 112-124. doi:10.1016/j.lithos.2008.10.021.

[61] Priestley, K., McKenzie, D., Debayle, E., Pilidou, S., 2008. The African upper mantle and its relationship to tectonics and surface geology, *J. Geophys. Int.,* 175, 1108-1126.

[62] Sebai, A., Stutzmann, E. , Montagner, J.-P., Sicilia, D., Beucler, E., 2006. Anisotropic structure of the African upper mantle from Rayleigh and Love wave tomography, Phys. Earth and Planet. Int., 155, 48-62.

[63] Smith, M. and P. Mosley, 1993. Crustal heterogeneity and basement influence on the development of the Kenya rift, Tectonics, 12, 591-606.

[64] Stark, C. P., Stewart, J., Ebinger, C. J., 2003. Wavelet transform mapping of the effective elastic thickness and plate loading: Validation using synthetic data and application to the study of the South African tectonics, J. Geophys. Res., 108(B12), 2558, doi:10.1029/2001JB000609.

[65] Storey, B., 1995. The role of mantle plumes in continental break-up: case histories from Gondwanaland, Nature, 377, 301-308.

[66] Swain, C. J., J. F. Kirby, 2003. The effect of 'noise' on estimates of effective elastic thickness of the continental lithosphere by the coherence method, *Geophy. Res. Lett., 30*, 1574 doi:10.1029/2003GL017070.

[67] Tappe, S. et al., 2007, Craton reactivation on the Labrador Sea margins: Ar-40/Ar-39 age and S-Nd-Hf-Pb isotope constraints from alkaline and carbonatite intrusives, Earth and Planet. Sci. Lett., 256, 433-454.

[68] Tessema, A., Antoine, L. A. G. , 2003. Variation in effective elastic plate thickness of the East Africa lithosphere, *J. Geophys. Res., 108*, doi:10.1029/2002JB002200.

[69] Watts, A.B., 1982. Tectonic subsidence, flexure and global changes of sea-level, Nature, 297, 469-474.

[70] Watts, A.B., S. Lamb, J. D. Fairhead and J. F. Dewey, 1995, Lithospheric flexure and bending of the Central Andes, Earth Planet. Sci. Letts., 134, 9-21.

[71] Watts, A. B., 2001, Isostasy and Flexure of the Lithosphere, Cambridge University Press. 472 pp.

[72] Wang, Y., Wen, Y. and D. Weidner, 2008. Upper mantle SH- and P-velocity structures and compositional models beneath southern Africa, Earth Planet. Sci. Lett., 267, 596-608.

[73] Weertrane, D. S., Forysth, D. W., Fischer, K. M., Nyblade, A. N., 2003. Evidence for an upper mantle plume beneath the Tanzanian craton from Rayleigh wave tomography, J. Geophys. Res., doi:10.1029/2002JB002273.

[74] Whaler, K., Hautot, S. 2006, The electrical resistivity structure of the crust beneath the northern Ethiopian rift, in *The Structure and Evolution of the East African rift system in the Afar volcanic province*, edited by G. Yirgu, C. J. Ebinger, and P. K. H. Maguire, Geol. Soc. Spec. Publ., 256, 294-305.

[75] Whitehouse, P., Latychev, K., Milne, G. A., Mitrovica, J. X., Kendall, R., 2006. Impact of 3-D Earth structure on Fennoscandian glacial isostatic adjustment: Implications for space-geodetic estimates of present-day crustal deformations, Geophys. Res. Lett., 33, doi:10.1029/2006GL026568.

[76] Wolfenden, E., Ebinger, C., Yirgu, G., Deino, A., Ayalew, D., 2004. Evolution of the northern Main Ethiopian rift: birth of a triple junction, Earth and Planet. Sci. Lett., 213-228.

[77] Kirby, J.F., and C.J. Swain (in press). A reassessment of spectral Te estimation in continental interiors: the case of North America, Journal of Geophysical Research, doi: 10.1029/2009JB006356.

[78] Macario, A., Malinverno, A. and W. F. Haxby, 1995, On the robustness od elastic thickness estimates obtained using the coherence method, J. Geophys. Res., 100(D8), 15,163-15,172.

[79] Kalnins, L. M., and Watts, A. B., 2009, Spatial variations in effective elastic thickness in the Western Pacific Ocean and their implications for Mesozoic volcanism, Earth Planet. Sci. Lett., 286(1-2), 89-100, doi:10.1016/j.epsl.2009.06.018.

[80] Frederik J. Simons and Rob D. van der Hilst, Seismic and mechanical anisotropy and the past and present deformation of the Australian lithosphere, Earth & Planetary Science Letters, 2003, 211 (3-4), 271-286, doi:10.1016/S0012-821X(03)00198-5

Appendix A

A fundamental assumption of the load deconvolution method developed by Forsyth (1985) is that surface and subsurface loads are statistically uncorrelated. Subsurface loads include mafic intrusions, accreted lower crustal material, thermal anomalies and/or compositional variations. Macario et al. (1995) showed (unsurprisingly) that statistical correlation of surface and subsurface loads leads to a bias in the T_e values obtained using Forsyth's (1985) method. Statistical correlation between surface and subsurface loads arises when they are in phase, i.e. when they have some systematic relationship to each other. This may occur e.g. where magmatic intrusions occur directly beneath volcanic edifices, as may be the case throughout the East African and Main Ethiopian rifts, the Afar depression and the intra-continental

volcanic provinces of Africa. In this appendix we demonstrate that although load correlation occurs in some of these areas in Africa, it is only significant at wavelengths $\sim< 100$ km and it does not affect the our T_e estimates.

We start by defining the Bouguer coherence as:

$$\gamma^2 = \left\langle \frac{GH^* *(GH^*)^*}{GG^* * HH^*} \right\rangle$$

where G and H are the Fourier transforms of the Bouguer gravity anomaly and topography, * indicates complex conjugation and the brackets indicate annular wavenumber bin averaging. Note that, differently than here, in the classical definition of coherence the averaging in annular wavenumber bins is done prior to the division of the numerator by the denominator in eq. 1 (see for comparison eq. 3 in Kirby and Swain, 2009). The effect of averaging the quotients is to increase the level of the coherence at short wavelengths, so that the coherence curve flattens out at around 0.1 instead to 0, but it does not change the position of the roll-over of the coherence (the wavelengths at which the coherence increases from 0 to 1), nor the final estimate of T_e.

Kirby and Swain (2009) present an extensive analysis of load correlation and its effect on T_e using the load deconvolution method of Forsyth (1985). These authors have shown that load correlation can be identified in the Bouguer complex coherency (see their figure A2a). Here we define the coherency as:

$$\Gamma = \left\langle \frac{GH^*}{\sqrt{GG^*} * \sqrt{HH^*}} \right\rangle,$$

consistent with our definition of coherence (compare with eq. 5 in Kirby and Swain, 2009). We have tested against simulated data to ensure that our slightly different averaging scheme for the coherency does not change the results. As Kirby and Swain (2009) point out, because the product GH^* is complex, the coherency is a complex variable, $\Gamma = \Gamma_R + i\Gamma_I$, and therefore contains information that the coherence (a real-valued function) does not. Particularly, the phase of the coherency, $\varphi = \tan^{-1}\left(\frac{\Gamma_I}{\Gamma_R}\right)$ measures the phase difference after flexure between surface and subsurface loads (Kirby and Swain, 2009). Kirby and Swain (2009) also show that the real part of the Bouguer coherency identifies wavelengths over which loads are correlated (see their Figure A2). This result is replicated in our Figure A1, showing the recovered T_e, the Bouguer coherence, γ_B^2, and the real part of the Bouguer coherency, Γ_{RB}, along a profile at x = 1750 km for three synthetic topography and Bouguer gravity anomaly data sets of 5100x5100 km dimension with a 20 km grid spacing. The window sizes used for calculation of the coherence, coherency and T_e are 2000x2000 km. The data sets have been generated with varying amounts of correlation of the *a priori* loads. In the synthetic data the correlation coefficient, R (see definition below), is constant over all wavelengths. The figures also show the coherence transition wavelength for the (20 km) T_e with which the data were generated (dashed black line). To construct the two initially correlated load surfaces, u and v', we followed Macario et al. (1995) and Kirby and Swain (2009). We first generate two random, fractal surfaces, u and v which are uncorrelated. A further surface, v', was generated which is correlated by an amount R, the correlation coefficient, with the surface load u, by:

$$v' = Ru + v\sqrt{1-R^2}$$

We use positive correlation coefficients $R = 0.33$ and $R = 0.66$, as distinct from the negative coefficients used by Macario et al. (1995) and Kirby and Swain (2009). The reason for this is that correlated loads in African volcanic provinces appear to be positively correlated, as will be shown shortly. Figure A1 shows that when initial loads are positively correlated at all wavelengths, the real part of the Bouguer coherency exceeds zero at wavelengths smaller than the transition wavelength (dashed black line). It also shows that as the correlation coefficient increases, the T_e is overestimated. Macario et al. (1995) and Kirby and Swain (2009) demonstrated that T_e is underestimated when initial loads are negatively correlated, so in fact T_e can be either over- or under-estimated depending on the sign of the correlation, as previously suggested by Kirby and Swain (2009).
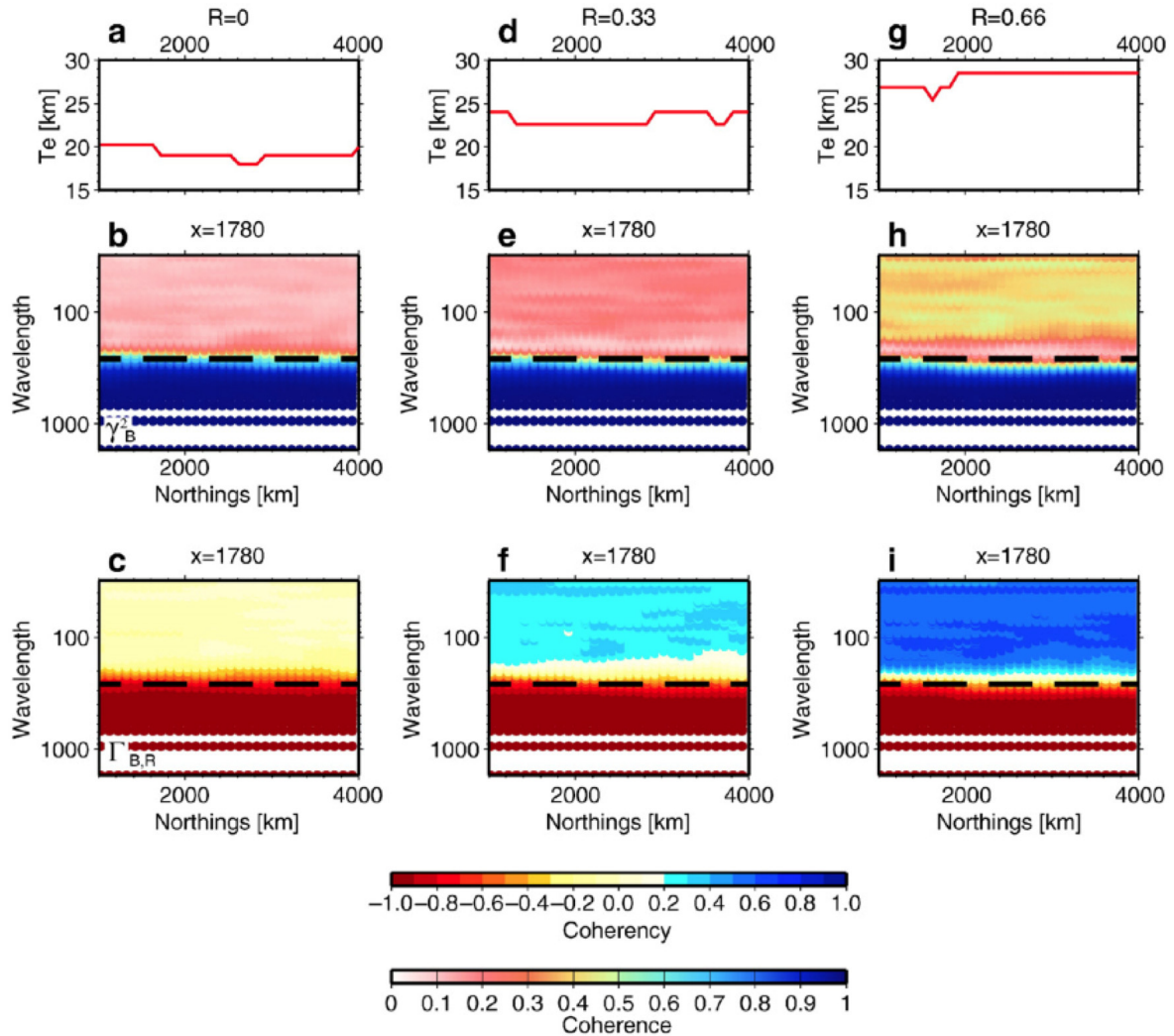
_____

Figure A1. Estimated T_e (first row), Bouguer Coherence (second row) and real part of the Bouguer coherency (third row) of three synthetic data sets generated with different correlation coefficients, R, at all wavelengths. The synthetic data sets consist of topography and Bouguer anomaly generated with a T_e of 20 km, and are 5100x5100 km with a grid spacing of 20 km. The figure shows the coherence along all northings with easting: x=1750 km. Figures A1a, b, and c show results for $R = 0$; Figures A1d, e and f show results for $R = 0.33$; and Figures A1g, h and i show results for $R = 0.66$. Note how T_e is overestimated as the degree of correlation increases. T_e is underestimated when the correlation coefficient between the initial loads is negative (Macario et al., 1995; Kirby and Swain, in press, 2009).

_____

However, in nature loads may not be correlated over all wavelengths. For example, volcanic edifices are normally less than 100 km in diameter, so a potential correlation of volcanic surface loads with subsurface magmatic intrusions may occur at wavelengths less than ~100

km. Figure A2 shows the same quantities as Figure A1 but in this case the synthetic topography and gravity anomaly data have been generated with initial loads that are correlated at wavelengths < 100 km. Over a waveband from 100-120 km loads are decreasingly correlated and at wavelengths > 120 km no initial load correlation exists. The correlation parameters are otherwise identical to the previous experiment. The figure shows that for a T_e of 20 km and an estimation window of 2000x2000 km, T_e estimates are unaffected by load correlation. This is because the transition wavelength of the Bouguer coherence is greater than the waveband over which the correlation occurs. The figure also shows that the real part of the Bouguer coherency delimits very well the waveband over which the loads are correlated. We tested that the real parts of the Bouguer coherency delimit well the waveband over which the correlation occurs for other T_e values to confirm that this is true independent of T_e. Therefore we apply this quantity to evaluate load correlation in Africa.
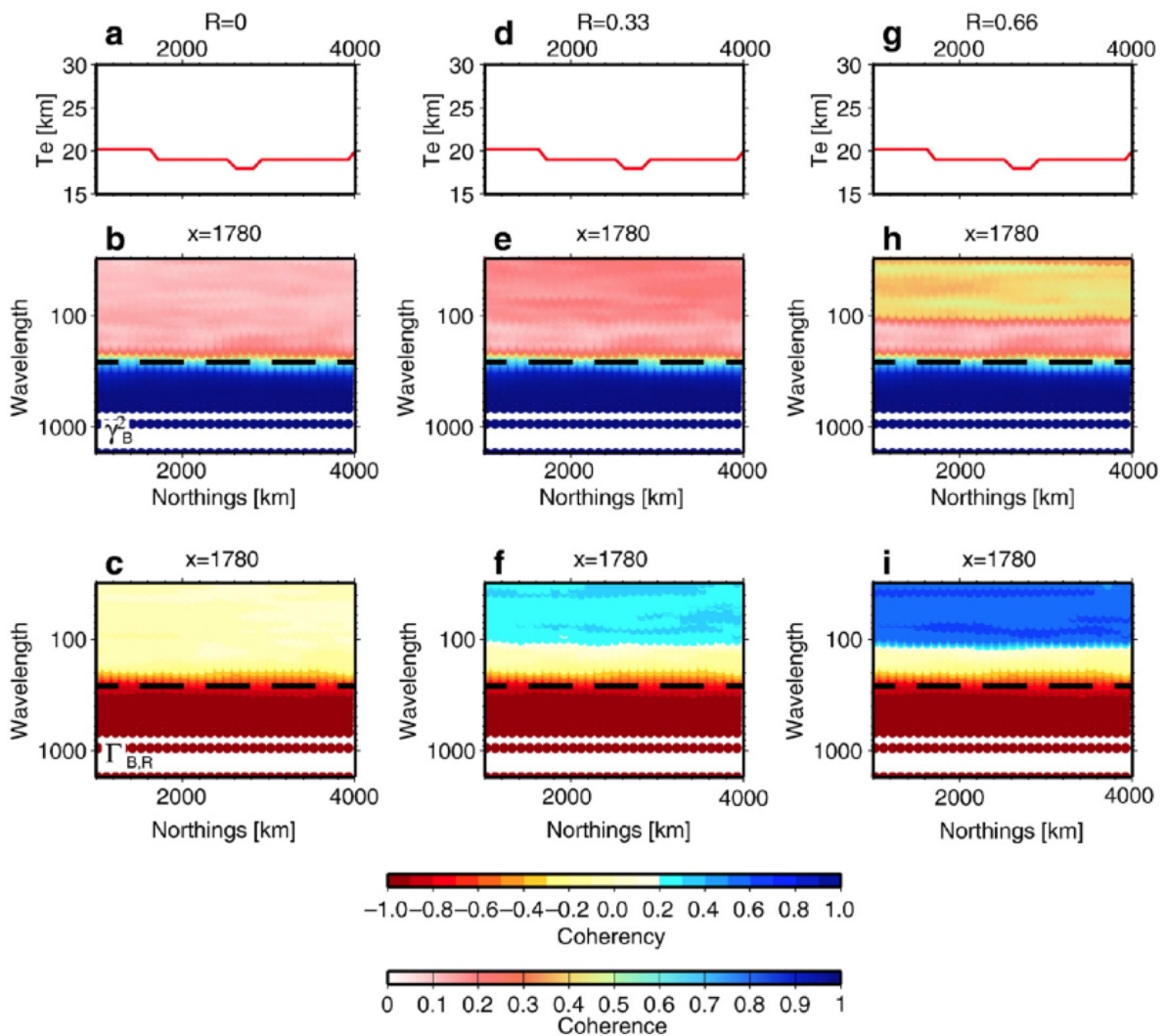
_____

Figure A2. Estimated T_e (first row), Bouguer Coherence (second row) and real part of the Bouguer coherency (third row) of three synthetic data sets generated with different correlation coefficients between initial loads, R, at wavelengths < 100 km (see Appendix A for a detailed description). The synthetic data sets consist of topography and Bouguer anomaly generated with a T_e of 20 km, and are 5100x5100 km with grid spacing of 20 km. The figure shows the coherence along all northings with easting: $x = 1750$ km. Figures A1a, b, and c show results for $R = 0$; Figures A1d, e and f show results for $R = 0.33$; and Figures A1g, h and i show results for $R = 0.66$. Note how T_e does not change with increasing degree of correlation. This is because the waveband over which loads are correlated is less than the transition wavelength of T_e.

_____

Figure A3 shows a map of T_e of Africa calculated with 600x600 km windows (without bias correction for windowing) and in cartesian coordinates with the tracks along which we plot the topography, the Bouguer coherence and the real part of the Bouguer coherency in Figure A4. Note in Figure A4 that along any profile the wavelength of the Bouguer rollover changes as T_e increases or decreases along the track. Figure A4 demonstrates that positive load correlation does not occur in western Africa but exists in eastern Africa in the areas of the East African and Main Ethiopian rifts and Afar, but only at wavelengths < ~100 km (see e.g. locations x=6516, 7524 and 8028 km in the figure).
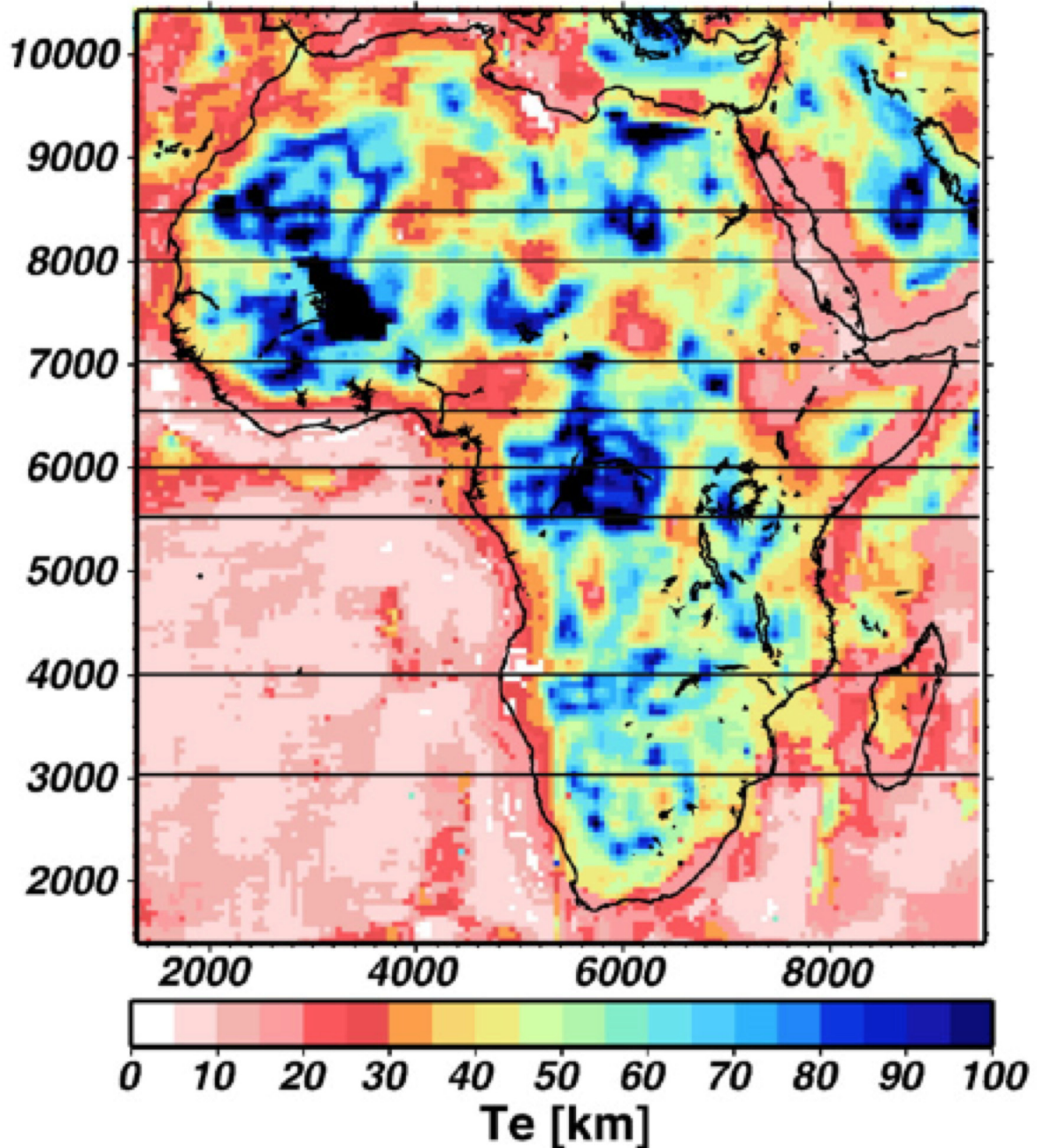
———————————————

Figure A3. Map of T_e of Africa calculated with 600x600 km windows (without bias correction for windowing) and in cartesian coordinates with the tracks along which we plot the topography, the Bouguer coherence and the real part of the Bouguer coherency in Figure A4.
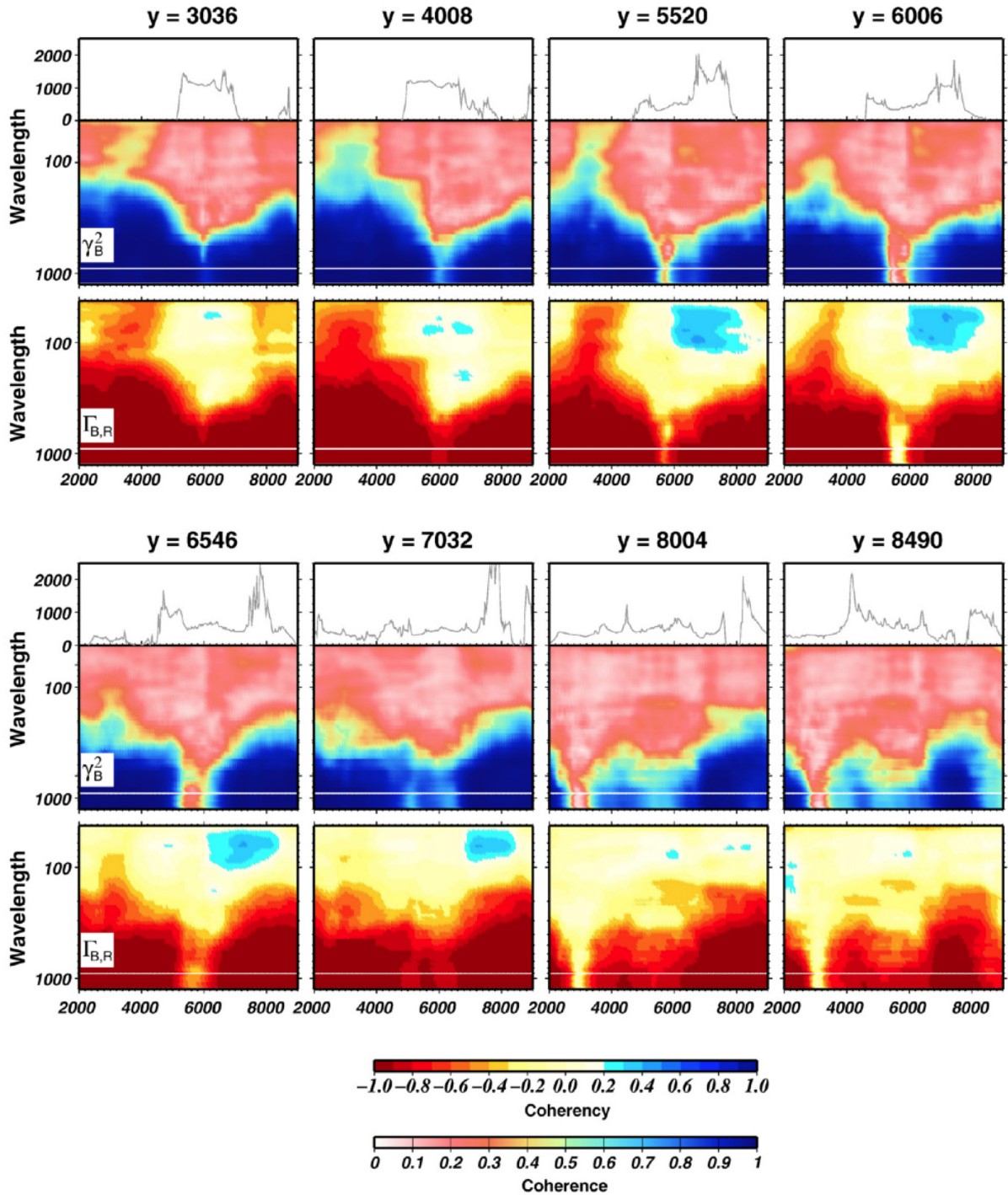
———————————————

_____

Figure A4. Shows at 8 different *x* locations in Africa (see Figure A3), the topography (first row), the Bouguer coherence (second row) and the real part of the Bouguer coherency (third row). The figure shows that positive load correlation does not occur in western Africa (compare with Figure A2) but exists in eastern Africa in the areas of the East African and Main Ethiopian rifts and Afar, but only at wavelengths < ~100 km (see locations *x* = 6516, 7524 and 8028 km in the figure). The windows to calculate the Bouguer coherence and real part of the Bouguer coherency are 2000x2000 km wide.

_____

To estimate the effect of this short wavelength correlation on our T_e estimates we compare in Figure A5 the mean estimate of T_e and its standard deviation from tests with 100 synthetic topography and Bouguer anomaly data sets generated with uncorrelated initial loads and input T_e of 10-200 km (identical to Figure 2) with the mean estimate of T_e and its standard deviation resulting from tests with synthetic data generated with loads that are initially

correlated ($R = 0.66$) at wavelengths <120 km (as previously described). The figure shows that regardless of the data window size used for analysis and the input T_e with which the data is generated, wavelength correlation at such short wavelengths does not affect our T_e estimates.
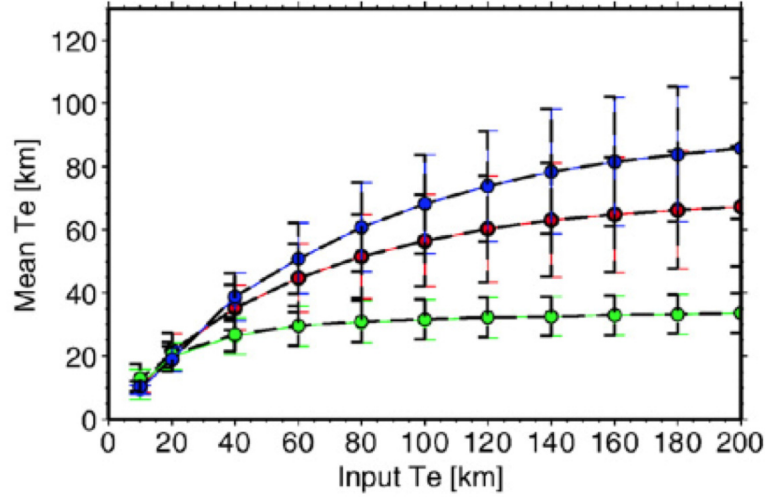
_____

Figure A5. Mean recovered T_e (circles) and its standard deviation, (error bars), resulting from 100 experiments with synthetic topography and gravity generated with a spatially constant input T_e and no correlation at any wavelength (blue, red and green colours identifying different window sizes for estimation, see below), superimposed with dashed black lines, which show the results for synthetic data with generated with initial loads correlated with an R of 0.66 at wavelengths <~100 km (see Appendix for data generation). Three windows for analysis are used: green line, 400x400 km; red line, 600x600 km windows; blue line, 800x800 km windows. The dashed black lines plot exactly on top of the coloured lines indicating that if initial load correlation is restricted to wavelengths < ~100 km (as observed in Figure A4), the estimated T_e is not biased for any estimation window nor input T_e value.